



**HAL**  
open science

# Change in Wind Renewable Energy Potential under Stratospheric Aerosol Injections

Susanne Baur, Benjamin M Sanderson, Roland Sférian, Laurent Terray

► **To cite this version:**

Susanne Baur, Benjamin M Sanderson, Roland Sférian, Laurent Terray. Change in Wind Renewable Energy Potential under Stratospheric Aerosol Injections. 2024. hal-04449996

**HAL Id: hal-04449996**

**<https://hal.science/hal-04449996>**

Preprint submitted on 9 Feb 2024

**HAL** is a multi-disciplinary open access archive for the deposit and dissemination of scientific research documents, whether they are published or not. The documents may come from teaching and research institutions in France or abroad, or from public or private research centers.

L'archive ouverte pluridisciplinaire **HAL**, est destinée au dépôt et à la diffusion de documents scientifiques de niveau recherche, publiés ou non, émanant des établissements d'enseignement et de recherche français ou étrangers, des laboratoires publics ou privés.

1 **Change in Wind Renewable Energy Potential under Stratospheric Aerosol Injections**

2 **Susanne Baur<sup>1</sup>, Benjamin M. Sanderson<sup>2</sup>, Roland Séférian<sup>3</sup>, Laurent Terray<sup>1</sup>**

3 <sup>1</sup>CECI, Université de Toulouse, CERFACS, CNRS, Toulouse, France

4 <sup>2</sup>Centre for International Climate and Environmental Research (CICERO), Oslo, Norway

5 <sup>3</sup>CNRM, Université de Toulouse, Météo-France/CNRS, Toulouse, France

6 Corresponding author: Susanne Baur (susanne.baur@cerfacs.fr)

7

8 **Key Points:**

- 9
- 10 • Stratospheric Aerosol Injections have been proposed as a method to temporarily counteract the warming from greenhouse gases.
  - 11 • Stratospheric Aerosol Injections do not compensate the atmospheric circulation changes from climate change but create new dynamics.
  - 12 • Total global wind energy potential is negligibly reduced under Stratospheric Aerosol Injections but regional trends can be large.
- 13
- 14
- 15

## 16 **Abstract**

17 Wind renewable energy (WRE) is an essential component of the global sustainable energy  
18 portfolio. Recently, there has been increasing discussion on the potential supplementation of this  
19 conventional mitigation portfolio with Solar Radiation Modification (SRM). However, the impact  
20 of SRM on conventional mitigation measures has received limited attention to date. In this study,  
21 we explore one part of this impact, the potential effect of one type of SRM, Stratospheric Aerosol  
22 Injections (SAI), on WRE. Using hourly output from the Earth System Model CNRM-ESM2-1,  
23 we compare WRE potential under a medium emission scenario (SSP245) and a high emission  
24 scenario (SSP585) with an SRM scenario that has SSP585 baseline conditions and uses SAI to  
25 cool to approximately SSP245 global warming levels. Our results suggest that SAI may affect  
26 surface wind resources by modifying large-scale circulation patterns, such as a significant  
27 poleward jet-shift in the Southern Hemisphere. The modeled total global WRE potential is  
28 negligibly reduced under SAI compared to the SSP-scenarios. However, regional trends in wind  
29 potential are highly variable, with large increases and decreases frequently reaching up to 16 %  
30 across the globe with SAI. This study provides valuable insights into the potential downstream  
31 effects of SRM on climatic elements, such as wind patterns, and offers perspectives on its  
32 implications for our mitigation efforts.

## 33 **1 Introduction**

34 Wind renewable energy (WRE) is a key component of the transition to a low-carbon energy  
35 system (IPCC, 2018; Clarke et al., 2022; Riahi et al., 2022). Modeling assessments estimate that  
36 in Paris Agreement compatible scenarios, such as the C1 and C2 scenarios from the recent IPCC  
37 Assessment Report (Riahi et al., 2022), a significant portion of energy would come from wind  
38 with projected production ranging from 4,760 to 50,960 TWh/yr by 2050 depending on the  
39 scenario and model (Byers et al., 2022). However, present policies are taking us closer to a global  
40 mean surface temperature increase of 2.5-2.9°C than the Paris compatible 1.5°C (CAT, 2023),  
41 whilst current warming already leads to numerous climate change related damages (Ripple et al.,  
42 2023). Hence, a growing number of people are investigating a group of technologies, termed Solar  
43 Radiation Modification (SRM), as a potential addition to conventional mitigation, to rapidly  
44 manage climate change risks. SRM does not resolve the global warming problem as it does not  
45 eliminate greenhouse gases (GHGs), but is proposed to temporarily mask some of the impacts with

46 the logic of providing more time to sufficiently roll out mitigation measures and halt or reverse the  
47 rise of atmospheric GHG concentration (Horton, 2015; MacCracken, 2009; Royal Society, 2011;  
48 Schäfer et al., 2014). It works by modifying the balance of incoming and outgoing radiation in the  
49 Earth system, which, if done on a significant scale, can exert a global cooling effect to counteract  
50 warming due to greenhouse gases. SRM is perceived controversially by experts and laypeople  
51 alike (Müller-Hansen et al., 2023) due, in part, to the large social and ecological risks and  
52 unknowns involved in intentionally manipulating the complex Earth system.

53 Various proposals have been put forward to alter the radiative equilibrium, with the  
54 injection of aerosols into the stratosphere (SAI) receiving the most attention thus far. An SAI  
55 intervention aiming at global impact entails the continuous placement of aerosols at low latitudes  
56 in the lower stratosphere (Dai et al., 2018; Kravitz et al., 2019a; Tilmes et al., 2017; Tilmes et al.,  
57 2018b), where the Brewer-Dobson circulation slowly transports them towards the poles. The  
58 aerosols reflect the incoming short-wave radiation allowing less radiative energy to reach the  
59 surface. While this process leads to cooling at the surface, evidenced by large volcanic eruptions,  
60 not all radiation is reflected by the aerosols. Instead, some of the radiative energy is absorbed by  
61 the particles, leading to localized heating of the stratosphere, which can affect global circulation  
62 patterns (Baldwin & Dunkerton, 2001; DallaSanta et al., 2019; Stenchikov et al., 2002; Graft et  
63 al., 1993). For example, several studies on the impact of stratospheric aerosols from volcanic  
64 eruptions have found a poleward jet shift (Barnes et al., 2016; Polvani & Kushner, 2002; Simpson  
65 et al., 2009). This has been attributed to two general mechanisms, surface cooling and stratospheric  
66 warming (DallaSanta et al., 2019). The surface cooling from the stratospheric aerosols decreases  
67 the tropospheric meridional temperature gradient (Stenchikov et al., 2002; Graf, 1992), which  
68 reduces midlatitude baroclinity, driving a strengthening of the stratospheric vortex, which leads to  
69 a poleward shift of the jet (Baldwin & Dunkerton, 2001). The second and primary mechanism,  
70 however, is the observed warming of the stratosphere in the tropics due to the aerosol's absorption  
71 of the radiative energy. This enhances the stratospheric meridional temperature gradient leading  
72 to a strengthened stratospheric vortex that shifts the jet poleward (DallaSanta et al., 2019).  
73 Modeling studies on SAI impacts have also found large-scale circulation changes. Liu et al. (2023)  
74 studied the East Asian Winter Monsoon under SAI and found that aerosol injections reverse the  
75 weakening of the monsoon that occurs in SSP585. In Africa, however, SAI can lead to weaker  
76 monsoon winds (Da-Allada et al., 2020; Robock et al., 2008) and a slight southward shift of the

77 ITCZ (Cheng et al., 2019). It should be emphasized that the outcomes of these studies are likely  
78 strongly reliant on the selected injection design and the underlying model (Kravitz et al., 2016,  
79 2019b; Lee et al., 2020; MacMartin & Kravitz, 2019).

80 Wind power generation relies significantly on local and regional wind patterns and even  
81 minor fluctuations in wind velocity can have a meaningful impact on the energy output (Veers et  
82 al., 2019). This is because the energy in the wind follows the cube of the wind speed. While to our  
83 knowledge no research has been conducted on WRE potential under SRM, several studies have  
84 looked at the impact of climate change on wind potential. They found significant alterations in  
85 wind velocity and its temporal distribution as a result of global warming (Solaun & Cerdá, 2019).  
86 One of the main mechanisms behind large-scale circulation changes from anthropogenic warming  
87 is the reduced equator-to-pole temperature gradient at the surface as a result from polar  
88 amplification, which is expected to alter tropical circulation (Ma et al., 2012), such as the Hadley  
89 cell, monsoon circulations and tropical cyclone frequency, as well as the behavior of midlatitude  
90 jet streams and storm tracks (Martinez & Iglesias, 2024; Pryor et al., 2020; Shaw et al., 2016).  
91 However, wind resources can be further impacted by ocean circulation and surface roughness  
92 changes from land cover modifications (Jung & Schindler, 2022; Vautard et al., 2010; Zeng et al.,  
93 2019). Additionally, local wind resources exhibit high variability on sub-hourly and multi-decadal  
94 scales (Jung et al., 2018). Due to the difficulty to accurately represent all drivers and the resulting  
95 temporal and spatial variations of wind patterns in Global Circulation Models, it is not entirely  
96 certain whether climate change will result in a decrease or increase in wind speeds at the global  
97 scale (Pryor et al., 2020). Most studies find highly diverse regional trends with large increases and  
98 decreases in wind speed and wind energy potential all over the globe (Gernaat et al., 2021; Jung  
99 & Schindler, 2022; Pryor et al., 2020; Solaun & Cerdá, 2019). As a result, on a global scale,  
100 changes in total wind energy density (Martinez & Iglesias, 2024) and wind energy potential  
101 (Gernaat et al., 2021) are small and may be slightly negative.

102 Given that WRE already plays an important role in the prevailing mitigation strategy, and  
103 that mitigation is an important aspect of ensuring the temporary use of SRM, it is important to  
104 understand whether SRM complements or conflicts with this existing method of energy generation  
105 and mitigation. Only through an understanding of the full spectrum of consequences from SAI can  
106 responsible decision-making be enabled. Here, we analyze the interplay between WRE and SAI

107 by calculating and comparing on- and offshore wind potential when SAI is used versus when  
108 mitigation has brought the climate to approximately the same GMST (SSP245). Additionally, we  
109 compare the SAI-modified climate with the fossil-fuel heavy emission baseline of the scenario  
110 without SAI (SSP585).

## 111 **2 Model Experiments and Methods**

### 112 2.1 Data and Simulations

113 This study is based on three experiments: a fossil-fuel intensive, high-emission scenario  
114 called SSP585 (O'Neill et al., 2016), a moderately ambitiously mitigated scenario, SSP245  
115 (O'Neill et al., 2016), and a stratospheric aerosol injection (SAI) simulation that cools down from  
116 an SSP585 baseline to SSP245. The SAI experiment originates from the GeoMIP6 protocol  
117 (Kravitz et al., 2015) and is referred to therein as G6sulfur. We run these experiments from 2015  
118 to 2100 in a 6-member ensemble with perturbed initial conditions on the CNRM-ESM-2.1 Earth  
119 system model (Séférian et al., 2019). Ensemble means are displayed except if defined otherwise.  
120 As a proxy for SAI we use prescribed aerosol optical depth derived from the GeoMIP G4SSA  
121 experiment (Tilmes et al., 2015) which scales up to 0.35 in the last decade of the simulation. The  
122 variables related to the directional winds  $u$  and  $v$  at 150m altitude are produced at hourly resolution  
123 on a  $1^\circ \times 1^\circ$  grid. During the postprocessing we bilinearly regrid the climate model output to match  
124 the land use and land cover data (described in 2.2.3 Politico-economic dimension) which is on a  
125  $0.1^\circ \times 0.1^\circ$  grid. For the zonal winds we create two altitudinal categories: upper and surface. Upper  
126 refers to a pressure level of 200-400hPa, roughly corresponding to the upper troposphere, and  
127 surface, referring to a pressure level of 850-1050hPa, representing the air close to the Earth's  
128 surface.

### 129 2.2 Wind Potential Calculation

130 In the same manner as Baur et al. (2023), we use the term “potential” to refer to an enhanced  
131 version of the traditional definition of the “technical potential”. The technical potential is the  
132 theoretical potential, here the surface wind resource, constrained by geographical and technical  
133 restrictions. In this study, we distinguish between three dimensions that are involved in the wind  
134 energy potential calculation: the technical dimension that establishes the technical restrictions to

135 the theoretical potential, the physical dimension, which is related to the energy extractable from  
 136 surface wind speed, and the politico-economic one, which is related to the suitability of the grid  
 137 cell  $i$  for wind turbine placement. We calculate the wind potential in a similar fashion to Gernaat  
 138 et al. (2021) as:

$$139 \quad TP_{i,loc} = Politicoeconomic_i \times Technical_{loc} \times Physical_{i,loc} \times gridcell_i \left[ \frac{MWh}{yr} \right] \quad (1)$$

140 All parameters, their values, units and sources are given in Table S1. The subscript  $loc$  indicates  
 141 whether it is an on- or offshore wind farm. The resulting electricity generation potential is  
 142 expressed in various time slices, such as 10-year seasonal mean changes, weekly sums and yearly  
 143 sums, calculated from the hourly wind speed input. Seasons refer to the four periods December,  
 144 January, February (DJF), March, April, May (MAM), June, July, August (JJA) and September,  
 145 October, November (SON). We calculate the Low Energy Week (LEW) metric as introduced by  
 146 Baur et al. (2023).

### 147 2.2.1 Technical Dimension

148 This part of the calculation reduces the physical potential by accounting for the  
 149 unavailability of the turbines due to maintenance, the wind farm array inefficiencies and the  
 150 density of wind turbine placement. We use technical indicators from on- and offshore exemplary  
 151 real-world wind turbines. To avoid projecting technological developments into the future we  
 152 choose turbines which are either already or about to be in serial production but are at the  
 153 forefront of current wind turbine development. We justify this choice with the argument that the  
 154 average wind turbines of the future will be the most powerful wind turbines of today. Table 1  
 155 lists their characteristics:

156 **Table 1.** Exemplary on- and offshore wind turbine specifications. Data from Vestas (2023a),  
 157 (2023b).

	Vestas V162-6.2 (onshore)	Vestas V236-15 (offshore)
<b>Rated power (<math>P_r</math>)</b>	6.2 MW	15 MW
<b>Cut-in windspeed (<math>v_{ci}</math>)</b>	3.0 m/s	3.0 m/s
<b>Cut-out windspeed (<math>v_{co}</math>)</b>	25 m/s	30 m/s

<b>Rotor diameter (<math>d_{Rotor}</math>)</b>	162 m	236 m
<b>Serial production</b>	2021	2024

158

159 The technical dimension consists of  $\eta_a$ , the annual availability of the turbine due to maintenance,  
 160  $\eta_{ar}$ , the wind farm array efficiency, and  $D_{loc}$ , the turbine density, and is a simple multiplication  
 161 of these terms:

$$162 \quad \text{Technical}_{loc} = \eta_a \times \eta_{ar} \times D_{loc} \left[ \frac{\text{turbines}}{\text{km}^2} \right] \quad (2)$$

163  $D$  is the average installed turbine density in the grid cell and is calculated as:

$$164 \quad D_{loc} = \frac{1}{(\text{spacing} \times d_{Rotor,loc})^2} \left[ \frac{\text{turbines}}{\text{km}^2} \right] \quad (3)$$

165 We assume that turbine spacing is equal in prevailing and perpendicular wind direction.  
 166 For the turbines set out in Table 1, this gives a  $D_{onshore}$  of 1.56 turbines/km<sup>2</sup> and a  
 167  $D_{offshore}$  of 0.51 turbines/km<sup>2</sup>. Translated into the more commonly used metric power  
 168 density, this implies 9.68 MW/km<sup>2</sup> onshore and 7.65 MW/km<sup>2</sup> offshore.

### 169 2.2.2 Physical Dimension

170 The physical dimension represents the power produced by a wind turbine  $p(v)$ , which is  
 171 described by the wind turbine power curve (Carrillo et al., 2013; Saint-Drenan et al., 2020; Fig S1)  
 172 and calculated as:

$$173 \quad p(v)_i = \begin{cases} 0 & v < v_{ci} \text{ or } v > v_{co} \\ q(v)_i & v_{ci} \leq v < v_r \\ P_r & v_r \leq v \leq v_{co} \end{cases} \quad (4)$$

174 The power curve depends on the instantaneous wind speed  $v$  and the characteristics of the wind  
 175 turbine (Table 1) and distinguishes between four different operation regimes (Fig S1): I, the area  
 176 of wind speeds ( $v$ ) that are smaller than the cut-in wind speed ( $v_{ci}$ ), and therefore too low to  
 177 produce any energy, II, the area of non-linear relationship between wind speed and power output  
 178 ( $q(v)$ ), III, the area of maximum power output, i.e. rated power ( $P_r$ ), and IV, the area after the cut-

179 out threshold, where wind speed is too high ( $v > v_{co}$ ) and turbines shut down to protect themselves  
 180 from damage (Saint-Drenan et al., 2020; Wood & Wollenberg, 1996).

181 Power production in area II follows the parametric wind turbine power curve described in Saint-  
 182 Drenan et al. (2020) and is calculated as:

$$183 \quad q(v_i) = 0.5 \times \rho \times \varepsilon_{loc} \times v^3 \times pc \left[ \frac{\text{MWh}}{\text{turbine}} \right] \quad (5)$$

184 With  $\rho$  being the air density, which is kept constant,  $\varepsilon$  the area swept by the rotor blades calculated  
 185 from the rotor blade diameters (Table 1),  $v$  instantaneous wind speed and  $pc$  the power coefficient,  
 186 a measure for aerodynamic-mechanical-electrical performance of the turbines (Veers et al., 2019).  
 187 For simplicity, in our study, the power coefficient is held constant, however, as demonstrated in  
 188 Saint-Drenan et al. (2020), it is ultimately dependent on and varies with the wind's velocity. The  
 189 power coefficient parameterization leads to a slight overestimation in power output from higher  
 190 wind speeds and underestimation of output from lower wind speeds in the  $q(v_i)$ -part of our  
 191 calculation.

192 Due to the high variability of wind, a temporal resolution of 1 hour and a spatial resolution  
 193 of  $1^\circ \times 1^\circ$  may not adequately represent all prevailing wind speeds in the area during the specified  
 194 time period. To account for the requirement of instantaneous wind velocity in the wind power  
 195 curve calculation and the low spatial resolution of the input data, we represent wind speed through  
 196 a probability density function. Weibull distributions have frequently been used to represent the  
 197 spread in wind speed over a time period at a given location (e.g. Aukitino et al., 2017; Mohammadi  
 198 et al., 2016; Shi et al., 2021; Shu et al., 2015) and as a means of downscaling to represent the  
 199 spread of wind over a larger area (Alizadeh et al., 2020; Chang et al., 2015; Tye et al., 2014; Zhou  
 200 & Smith, 2013). The temporal resolution of the underlying wind data can range from 10 min (Eskin  
 201 et al., 2008), to hourly (Chang et al., 2015; Li et al., 2020; Mohammadi et al., 2016; Burton et al.,  
 202 2001), 6-hourly (Elsner, 2019), to daily (Shu & Jesson, 2021) and longer. Cradden et al. (2014)  
 203 and Pryor et al. (2020) have highlighted the importance of a high temporal resolution of at least 1  
 204 hour for WRE analyses. Although hourly and daily average wind speeds have been shown to lead  
 205 to similar power output results from a turbine over a long time period, hourly input data is much  
 206 better at representing the peaks and lows during the day and can give a more precise result for  
 207 shorter time periods (Shin et al., 2018; Veronesi & Grassi, 2015; Justus et al., 1978). In this study,

208 the Weibull distribution is used to represent sub-grid spatial and temporal variation in wind. We  
 209 use a constant shape-parameter for all regions across the globe. This is a frequently applied  
 210 simplification (Dvorak et al., 2010; Elsner, 2019; Eureka et al., 2017; Shu et al., 2015; Sohoni et  
 211 al., 2016; Valencia Ochoa et al., 2019; Arendt et al., 2013) related to the width of the distribution  
 212 and therefore the gustiness of the wind regimes (Eureka et al., 2017) that is most commonly used  
 213 in larger scale analyses. Studies have demonstrated variation of the shape parameter across regions  
 214 (Zhou & Smith, 2013), especially for oceanic winds (Shi et al., 2021; Perrin et al., 2006). However,  
 215 apart from coastal areas, oceanic regions are excluded from this analysis and using the Rayleigh-  
 216 form of the Weibull distribution, which sets the shape parameter  $\beta$  to 2 and implies moderately  
 217 gusty winds across all areas (Eureka et al., 2017), drastically reduces the computational effort. The  
 218 scale parameter,  $\alpha$ , is calculated according to Lysen (1983) as follows:

$$219 \quad \alpha = ws_i \times (0.568 + 0.433 \times 0.5)^{\frac{1}{\beta}} \quad (6)$$

220 with  $ws_i$  being the hourly wind speed from our model output calculated as the square root of the  
 221 sum of the squares of the east- and northward wind components  $u$  and  $v$ . We calculate  $p(v)$  for all  
 222 1000 samples in the Weibull distribution for each 1 m/s wind speed bin from 0-50 m/s.  
 223 The 2-parameter Weibull distribution representing the range of wind speeds prevalent in the 1-  
 224 hour mean  $1^\circ$  grid cell model output is calculated as:

$$225 \quad f(T) = \frac{\beta}{\alpha} \times \left(\frac{T}{\alpha}\right)^{\beta-1} \times e^{-\left(\frac{T}{\alpha}\right)^\beta} \quad (7)$$

226 For computational feasibility we fit a curve between the 1-hour mean wind speed and the power  
 227 output, i.e.,  $p(v)$ , that takes into account the Weibull spread of wind speed and the turbine power  
 228 curve:

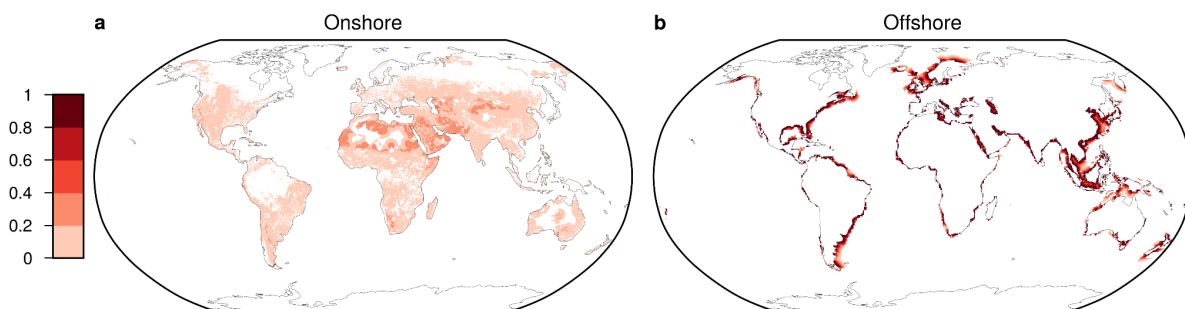
$$229 \quad Physical_{i,loc} = p(ws_i)_{loc} = a_{loc} \times \left(1 - e^{-\frac{ws_i^2}{b_{loc}}}\right) \times \left(1 - e^{-\frac{ws_i^2}{c_{loc}}}\right) \times e^{-\frac{ws_i}{d_{loc}}} \left[\frac{MWh}{turbine}\right] \quad (8)$$

230 Please consult Table S1 in the SI for the values of the parameters  $a_{loc}$ ,  $b_{loc}$ ,  $c_{loc}$  and  $d_{loc}$ . To  
 231 assess how much energy is lost due to a change in the distribution of hourly wind speeds we  
 232 additionally calculate the wind potential without the cut-out wind speed limit (no-cut-out). Instead,  
 233 power output at  $v > v_{co}$  is kept at  $P_r$ . By subtracting the yearly cumulative “standard”-turbine-

234 power-curve power output with the output from these no-cut-out calculations, we can estimate the  
 235 amount of TWh that is gained or lost in a year due to a change in fast winds. Figure S2 shows the  
 236 fitted power curve of an onshore and offshore grid cell in the normal setting and in the no-cut-out-  
 237 setting.

### 238 2.2.3 Politico-Economic Dimension

239 The incorporation of a politico-economic dimension is a long-standing approach for wind  
 240 potential calculations (e.g. Elliott & Schwartz, 1993; Archer & Jacobson, 2005; Bosch et al., 2017;  
 241 Hoogwijk, 2004; Zhou et al., 2012) and is related to the suitability of each grid cell to harbor wind  
 242 turbines. Various parameters have been taken into account in the past. Here, we consider surface  
 243 properties and land use competition for our onshore wind farms as done in Baur et al. (2023).  
 244 Figure 1 displays the convolutions of the single area restrictions for on- and offshore wind farms  
 245 which are used in the wind potential calculation ( $Politicoeconomic_i$ ). The single area restrictions  
 246 and their weights are displayed in Figure S3 and S4. We exclude all areas marked as protected  
 247 with any status as characterized by the United Nations Environment Programme (IUCN, 2023) as  
 248 possible wind power installation sites and weigh areas according to the prevalent land-use and  
 249 distance to highly populated centers as an indicator for the future existence of transmission lines  
 250 and demand. Highly populated areas are excluded since wind turbines are rarely situated in close  
 251 proximity to, or on top of, buildings. For offshore we add additional constraints, such as the  
 252 bathymetry over 1000m, exclusion of grid cells outside the Exclusive Economic Zone (EEZ)  
 253 (Flanders Marine Institute, 2019) and consideration of only those grid cells that are at least 95%  
 254 sea-ice free in every season of the year.



255  
 256 **Figure 1.** Convolution of area restrictions for a) onshore and b) offshore.

257 Land-use cover and population density data were obtained from the IMAGE3.0-LPJ model  
 258 (Doelman et al., 2018; Stehfest et al., 2014) with a spatial resolution of  $0.1^\circ \times 0.1^\circ$ . The model

259 differentiates between 20 different land use and land cover categories. We weigh each type  
260 according to the fraction of a grid cell that could be covered by wind farms, in line with Baur et  
261 al. (2023), but with different fractions assigned (see Table S2 for land use categories and assigned  
262 suitability fractions). The rationale behind the suitability fraction is that only part of a grid cell is  
263 available for wind farms as they could potentially conflict with other land uses such as cities,  
264 agricultural production or ecosystem services from forests. A suitability fraction of 15% denotes  
265 that 15% of the grid cell is able to accommodate a wind farm. The spacing between the turbines  
266 of several hundred meters enables a certain level of coexistence between wind farms and  
267 predominant land uses. This explains the assignment of higher fractions for, for example,  
268 agricultural areas in this study than in Baur et al. (2023), which looked at solar farms.

269 We use the same approach as Baur et al. (2023) to weigh the proximity to highly populated areas.  
270 The population data from the IMAGE3.0 LPJ model consists of 5-year intervals and is aggregated  
271 to 10-year means for our analysis (Doelman et al., 2018; Stehfest et al., 2014). Using a sigmoidal  
272 function, we impose that the weight diminishes proportionally as the distance to densely populated  
273 cells grows, ultimately tapering to zero at approximately 500 km. Unlike Baur et al. (2023), we  
274 exclude highly populated areas, which we define as cells where population density is larger than  
275 1000 inhabitants/km<sup>2</sup>.

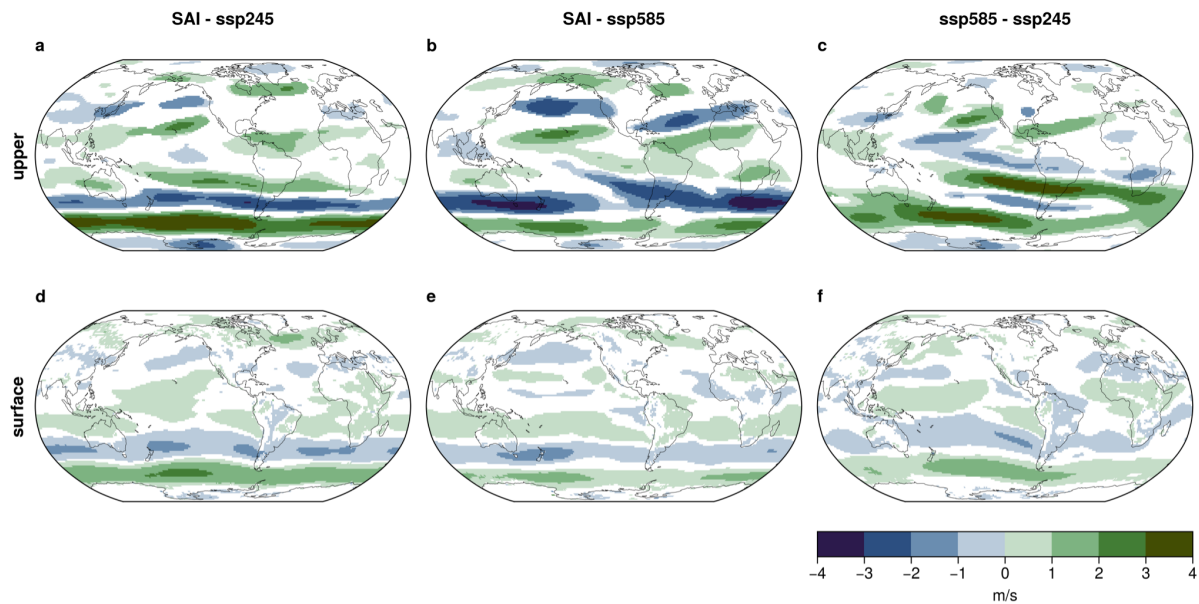
276  
277 We present results that are calculated using equal weights across all scenarios and time intervals.  
278 Therefore, the data underlying population, sea ice and land use are related to the 2090-2099 time  
279 frame of SSP245 but are used as a basis for all three scenarios.

## 280 **3 Results**

### 281 **3.1 Large-scale Circulation Response to SAI**

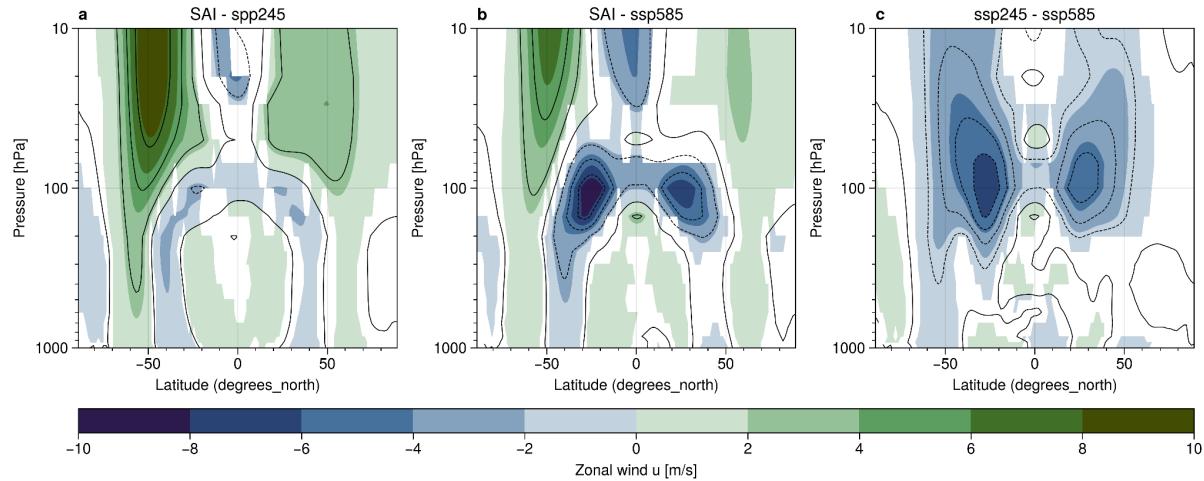
282 Our simulations indicate substantial alterations in 10-year mean zonal wind from the  
283 present (2015-2024) to the end of the century (2090-2099) (Fig S5). While the patterns of change  
284 show some similarities for SAI, SSP585 and SSP245, the magnitude of the circulation differences  
285 from present to future varies considerably and is especially pronounced for SAI and SSP585 (Fig  
286 S5). When comparing the future conditions of the scenarios with each other, substantial differences  
287 become apparent (Fig 2). Regardless of altitude or scenario-comparison, the largest differences are  
288 registered in the Southern Hemisphere (SH): Here, the westerlies' shift towards the pole is more

289 pronounced under SAI compared to the SSP-scenarios and, comparing the SSP-scenarios, there is  
 290 a more intense strengthening of the westerlies and poleward shift of the SH jet for SSP585  
 291 compared to SSP245 at the end of the century. The signal is strongest in the upper troposphere for  
 292 all scenario-comparisons with differences in zonal wind speed of up to 4 m/s (Figure 2 a-c). While  
 293 the sign of difference between SAI and the SSPs stays consistent across most seasons, the intensity  
 294 varies (Fig S6, S7).



295  
 296 **Figure 2.** Difference in 2090-99 mean zonal winds between a,d) SAI and SSP245, b,e) SAI and  
 297 SSP585 and c,f) SSP245 and SSP585 at a-c) the upper troposphere and d-f) the surface.

298 In the NH, the changes are less latitudinally and, over the Atlantic Ocean, altitudinally consistent.  
 299 While both upper tropospheric and surface winds show a pronounced equatorward shift of the  
 300 midlatitude westerlies over the Pacific under SAI compared to the SSPs, the upper troposphere  
 301 over the Atlantic entails a strengthened equatorward shift of the subtropical jet that does not  
 302 propagate as much to the surface as for the SH (Fig 2, 3, S5). The decrease in midlatitude wind  
 303 speed under SAI moves towards the equator as it propagates to the surface when comparing to  
 304 SSP245, while shifting slightly poleward when comparing to SSP585 (Fig 3 a,b). The largest  
 305 circulation changes occur in the upper troposphere and stratosphere (Fig 2, 3).

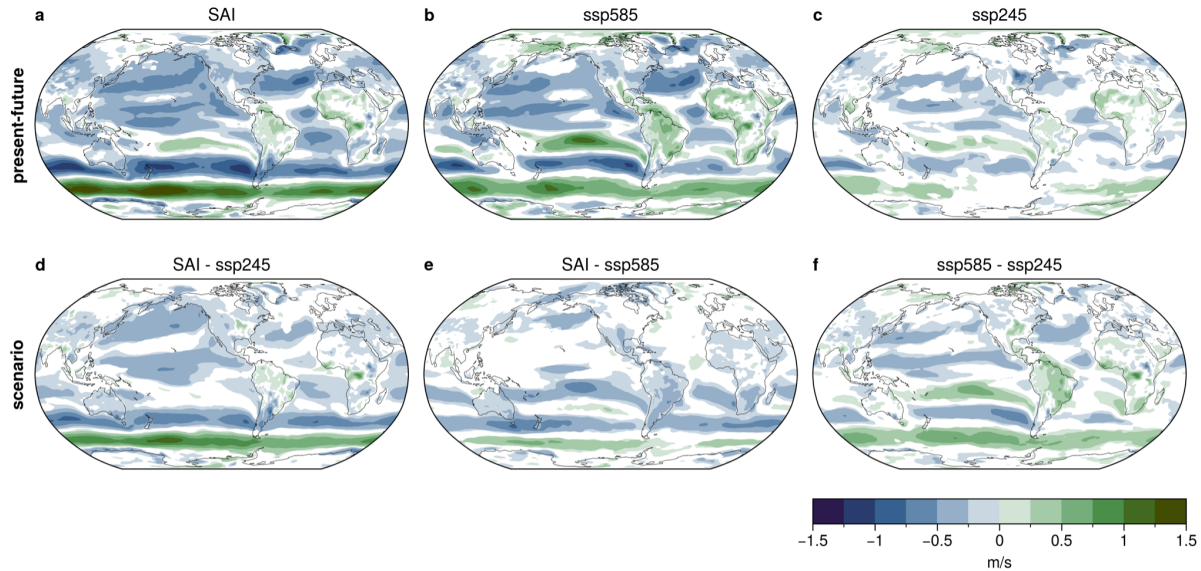


306

307 **Figure 3.** Difference in 2090-99 average zonal mean winds between a) SAI and SSP45, b) SAI  
 308 and SSP585 and c) SSP245 and SSP585.

309 Variation in large-scale circulation has been attributed to temperature changes in the stratosphere  
 310 and resulting increases or decreases in the temperature gradients at the surface and/or the upper  
 311 troposphere (Baldwin & Dunkerton, 2001; Charlesworth et al., 2023; DallaSanta et al., 2019;  
 312 Simpson et al., 2019; Stenchikov et al., 2002; Graf, 1992). In our simulations we see a large  
 313 temperature shift of up to 14K under SAI compared to the SSP-scenarios in the tropical  
 314 stratosphere (Figure S8). The largest increase is at around 80hPa. As expected, temperatures at the  
 315 surface are lower under SAI than SSP585, especially in the tropics, which is a common  
 316 phenomenon observed in SRM simulations. Due to the augmented CO<sub>2</sub> concentration, which  
 317 increases the rate that the stratosphere radiates heat to space, the stratosphere is colder under  
 318 SSP585 than SSP245 (Figure S8c).

319 Long-term average wind speed is substantially lower in the NH under SAI compared to the present  
 320 (Fig 4a) and compared to the SSPs (Fig 4d,e). A trend fairly consistent throughout the scenarios  
 321 but most noticeable in SSP585 is the increase in wind speed in tropical land regions compared to  
 322 the present, especially in Brazil and on the African continent. Most other land regions experience  
 323 reductions in wind speed (Fig 4a-c).



324

325 **Figure 4.** 150m wind speed comparing present (2015-2024) and future (2090-2099) states under  
 326 a) SAI, b) SSP585 and c) SSP245 and comparing future states of scenarios d) SAI and SSP245, e)  
 327 SAI and SSP585 and f) SSP585 and SSP245.

328

### 3.2 SAI effect on onshore and offshore wind potential

329

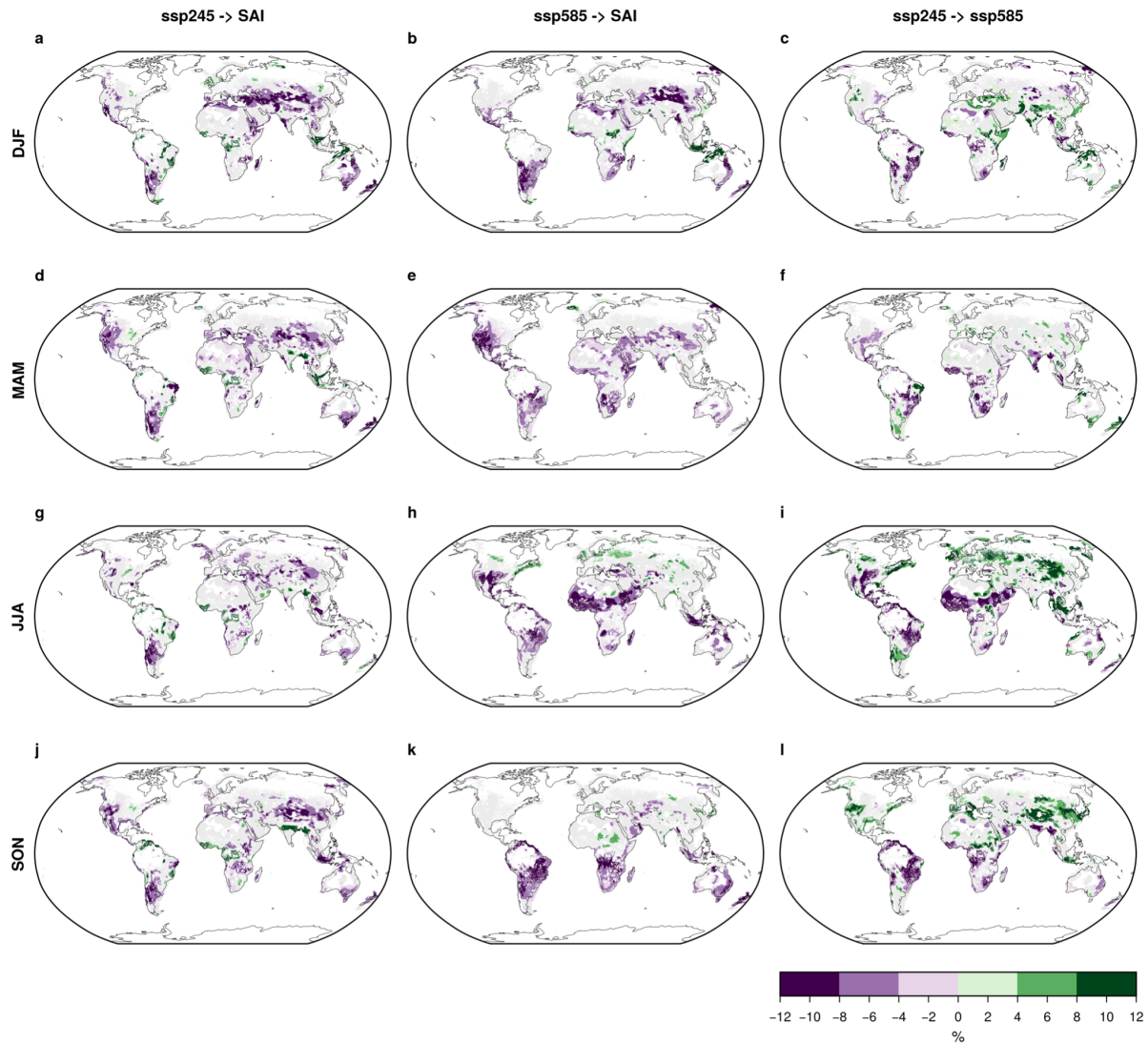
Results in this part are presented with respect to three different areas of interest: long-term  
 330 relative seasonal changes, changes in extended low-energy periods (LEW) and the effect of  
 331 changes in high hourly wind speed on annual energy production.

332

Figure 5 displays the relative difference in 2090-99 seasonal wind potential between the SSP-  
 333 scenarios and SAI (see Figure S9 for 10-year mean present to future comparisons for each  
 334 scenario). The sign of change is relatively consistent, although varying in strength, through the  
 335 different seasons for SSP245 -> SAI, except for the South East Asian and Northern European  
 336 region, where DJF and MAM show a large increase in wind potential, while JJA and SON show a  
 337 decrease (Fig 5a,d,g,j). The same seasonal pattern is visible for SSP585 -> SAI in South East Asia,  
 338 but not in Europe. In general, the seasons appear to agree less on the sign of the relative change  
 339 between SSP585 and SAI than for SSP245 and SAI. For example, apart from Europe and South  
 340 East Asia, also Central Africa and Central Asia show different trends depending on the season  
 341 when comparing SSP585 with SAI (Fig 5b,e,h,k). While there is not one single region that stands  
 342 out with especially large differences compared to others, the most pronounced differences in  
 343 SSP585 to SAI of around 16% are the large decrease in JJA in the southern Sahara (Fig 5h), the  
 344 decrease in northern China in DJF (Fig 5b), the decrease in South America through all seasons but  
 345 especially in Brazil in SON (Fig 5k) and Argentina, Bolivia and Paraguay in DJF (Fig 5b) and the

346 increase in South East Asia and the Chad and Sudan area in the south-east of the Sahara desert in  
347 DJF (Fig 5b). For SSP245 to SAI, Central Asia sees a significant decrease through all seasons but  
348 especially in DJF (Fig 5a). DJF furthermore indicates a large increase for southern South East  
349 Asia, northern offshore Australia and Central and South-East Brazil (Fig 5a). In MAM, East Brazil  
350 shows a big decreasing signal (Fig 5d). The SON months see a large increase in potential under  
351 SAI for Myanmar and Central/North India (Fig 5j). While the regional differences are diverse and  
352 large, globally, relative differences are small. SAI potential is only 2.2 % lower onshore and 1.3  
353 % lower offshore than for SSP245 and 3.0 % lower onshore and 0.9 % lower offshore than for  
354 SSP585. Between the SSP-scenarios the total global relative difference ends up being 0 % since  
355 onshore potential is increased under SSP585 compared to SSP245 by 0.6 % but onshore potential  
356 decreased by 0.6 %.

357



358

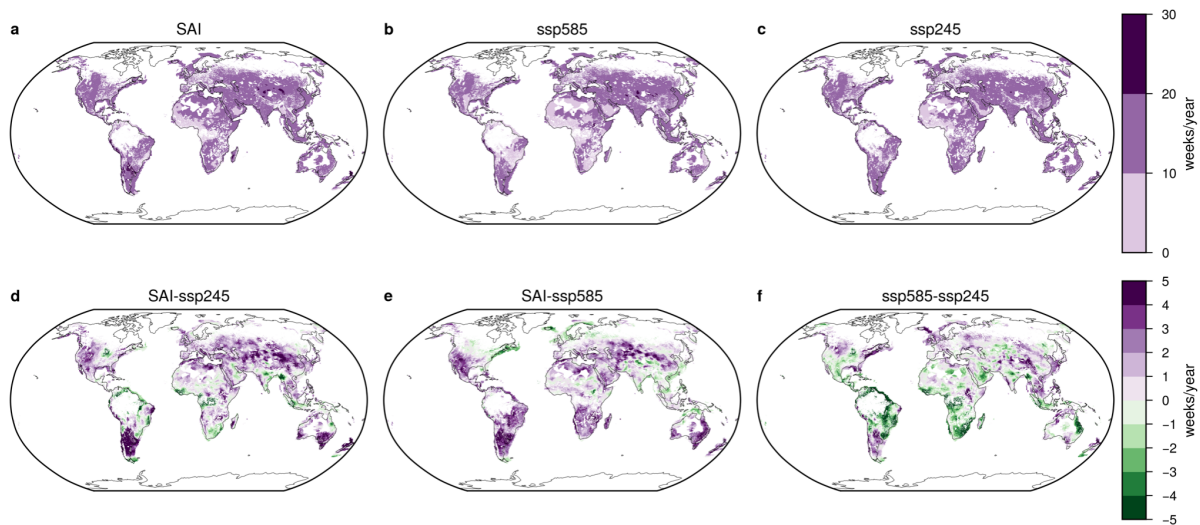
359 **Figure 5.** Relative differences in seasonal 2090-2099 wind potential for a,d,g,j) SSP245 to SAI,  
 360 b,e,h,k) for SSP585 to SAI and c,f,i,l) for SSP245 to SSP585 in the seasons a-c) December, January,  
 361 February (DJF), d-f) March, April, Mai (MAM), g-i) June, July, August (JJA) and j-l) September,  
 362 October, November (SON). Colored areas are statistically significant  $p < 0.05$ , gray areas are  
 363 considered suitable for wind production but show no significant change.  $x \rightarrow y$  denotes  $(y - x)/x$ .

364

365 The LEW metric assesses which regions experience prolonged periods of particularly low energy  
 366 production. Figure 6 displays the number of weeks per year in SAI, SSP585 and SSP245 that have  
 367 a wind energy output below the current (2015-2024) 20th seasonal percentile. Areas with up to 10  
 368 weeks per year imply that they stay unchanged in terms of low energy weeks or have less than in  
 369 the present. Apart from some small areas in central South America and central China, globally,  
 370 most areas see a slight increase in LEWs regardless of the scenario. West Africa, parts of the

371 Arabian Peninsula and south-east Brazil see no change or a decrease in LEWs in all scenarios.  
 372 However, when comparing the scenarios with each other and refining the color-coding, substantial  
 373 differences become apparent (Fig 6d-f). SAI leads to an increase of more than 6 additional LEWs  
 374 per year compared to SSP245 or SSP585 in large parts of southern South America, south-east  
 375 Australia, Central Asia and the Middle East. At the same time, many regions see less LEWs with  
 376 SAI than with the SSP-scenarios. For example, compared to SSP245, the Great Plains in the US,  
 377 several areas in Brazil, South Africa, West Africa, parts of the Arabian Peninsula, Myanmar and  
 378 India and north-east Australia seem to benefit from SAI in terms of LEW count. Compared to  
 379 SSP585, SAI appears to be especially advantageous in the north-east of North-America, northern  
 380 Europe, the Arafura and Timor Sea between Australia and Indonesia/Timor and some regions in  
 381 central China.

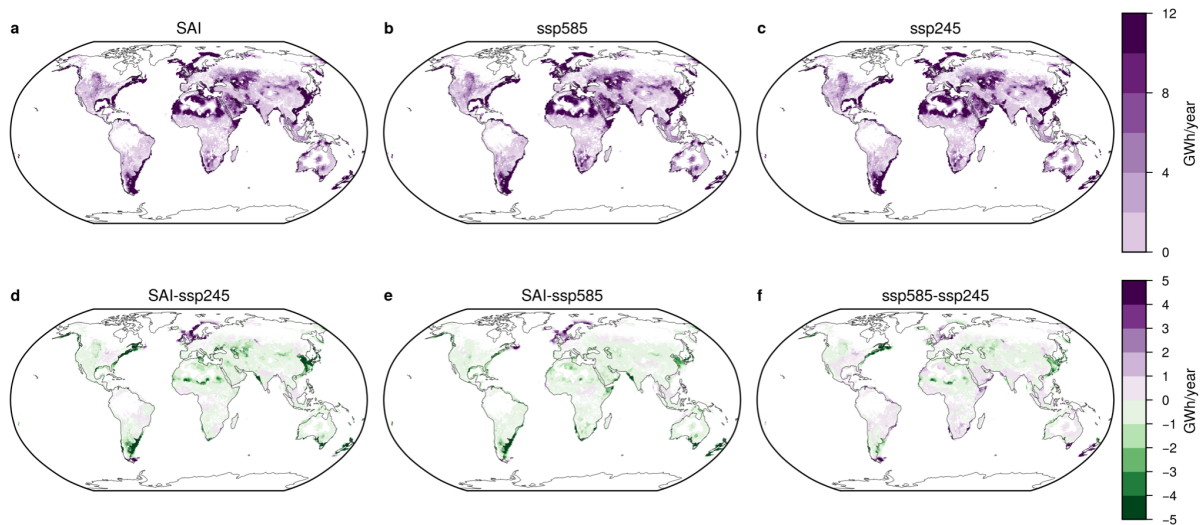
382 With some exceptions, such as north-east Australia, South Africa, northern Russia, offshore north-  
 383 east North America and offshore Indonesia, the sign and magnitude of change stays consistent  
 384 with the LEWs and the 10-year averages for SAI compared to SSP245 (Fig 6d, S10a). Similar for  
 385 SAI versus SSP585, where exceptions are in the offshore area of north-east North-America,  
 386 Mexico and southern US, offshore Borneo, Myanmar and South America, especially Argentina  
 387 (Fig 6e, S10b).



388  
 389 **Figure 6.** Low Energy Week (LEW) metric for a) SAI, b) SSP585 and c) SSP245. The LEW is  
 390 calculated between the present (2015-2019) and the future (2095-2099). See Baur et al. (2023) for  
 391 the LEW equation. d-f) are the differences between a-c).

392

393 To evaluate how much of the changes in wind potential are caused by changes in fast wind speed,  
 394 we measure the annual power loss resulting from winds exceeding the cut-out threshold. Figure 7  
 395 shows which areas are mostly affected by energy losses due to fast winds in GWh per year per  
 396 grid cell. Unsurprisingly, offshore areas are mostly affected by losses due to fast winds since wind  
 397 is generally significantly slower over land areas (Fig 7a-c) and we applied lower suitability  
 398 restrictions on offshore than onshore grid cells. Nevertheless, there are several onshore areas that  
 399 see substantial reductions, such as the Great Plains in the US, the Southern parts of the Sahara,  
 400 Central Asia and Russia. The differences between the scenarios are displayed in Figure 7d-f.  
 401 Offshore northern Europe, the tip of Argentina and eastern Canada are the only regions that have  
 402 substantially higher losses due to fast winds under SAI than the SSP-scenarios. SAI makes winds  
 403 offshore of China, eastern USA, New Zealand and south-east South America and, onshore, the  
 404 Sahara more accessible to energy generation. The total global energy loss due to fast winds is  
 405 lowest for SAI with 8.5 PWh/yr (2.6 %) and identical for SSP245 and SSP585 with 8.9 PWh/yr  
 406 (2.7 %).



407

408 **Figure 7.** Difference between normal power curve setting and “no-cut-out” power curve setting  
 409 for a) SAI, b) SSP245 and c) SSP585. Differences in energy lost due to fast winds between a) SAI  
 410 and SSP245, b) SAI and SSP585 and c) SSP585 and SSP245.

#### 411 4 Discussion

412 In this study, we examined the interplay between Stratospheric Aerosol Injections (SAI)  
 413 and renewable wind energy potential. We found large changes in wind potential under SAI  
 414 compared to a medium emission (SSP245) or high emission (SSP585) climate state depending on

415 the season and region (Fig 5, 6). The change in potential under SAI is especially regionally highly  
416 diverse with magnitudes frequently reaching 16 %. These large regional differences average out  
417 to a total global potential that is slightly smaller than for SSP245 or SSP585.

418 Wind energy potential is highly dependent on wind resources and long-term changes therein are  
419 mainly due to large-scale atmospheric circulation (Jung & Schindler, 2022). Previous analyses on  
420 stratospheric aerosols and atmospheric circulation have found impacts on global and regional  
421 circulation patterns, in particular a poleward shift of the jet (Barnes et al., 2016; McCusker et al.,  
422 2014; Polvani & Kushner, 2002; Simpson et al., 2009, 2019). In our analysis, we also found  
423 significant differences in zonal wind between SAI and the SSP-scenarios, as well as under the  
424 SSP-scenarios themselves (Fig 2, 3). The largest disparities exist within the Southern Hemisphere  
425 (SH) westerlies, which show a poleward shift under SAI compared to the SSP-scenarios, leading  
426 to both an increase and a decrease in the zonal mean wind of up to 4 m/s (Figure 2, 3). Our results  
427 are in agreement with those of Simpson et al. (2019), who studied alterations in large-scale  
428 circulation patterns using an SAI-setup known as GLENS. GLENS uses SAI to stay at 2020  
429 conditions under an SSP585 baseline (Tilmes et al., 2018a). Simpson et al. (2019) conducted  
430 separate isolated forcing experiments to analyze how shifts in zonal wind patterns are driven by  
431 the stratospheric temperature change from SAI in GLENS. The authors note westerly stratospheric  
432 anomalies in the extra-tropics of similar magnitude and pattern as those identified in our study,  
433 and attribute the dominant role driving this change in the SH to the heating of the tropical lower  
434 stratosphere, an effect likewise observed in our experiments (Figure S8). Studies on stratospheric  
435 aerosols from volcanic eruptions and circulation anomalies have made the same observation  
436 (Barnes et al., 2016; DallaSanta et al., 2019; Karpechko et al., 2010; McGraw et al., 2016; Graft  
437 et al., 1993; Kirchner et al., 1999) and attribution to stratospheric heating (Barnes et al., 2016;  
438 DallaSanta et al., 2019; Polvani & Kushner, 2002; Simpson et al., 2009). However, not all volcanic  
439 modeling results lead to the same conclusion: In the Northern Hemisphere (NH), Ramachandran  
440 et al. (2000) and Marshall et al. (2009) find an equatorward shift in response to the volcanic forcing  
441 instead and in the SH Robock et al. (2007) and Roscoe & Haigh (2007) found no or a slight  
442 equatorward shift. Simpson et al. (2019) and McCusker et al. (2015) observe, and our study  
443 confirms, that the SH shows a much stronger signal, and that not all the changes in the NH are  
444 attributable to the stratospheric heating, such as, for example, in the North Pacific or the Atlantic  
445 during JJA (Simpson et al., 2019).

446 Tang et al. (2023) noted a total global reduction in onshore wind speed as a side effect of SAI  
447 using the same underlying scenarios as this study, but a different model and a lower temporal  
448 resolution. They see similar spatial patterns and magnitudes of change in surface wind speed as  
449 we do (Fig 51-k in Tang et al., 2023), especially over land (Fig 4e), and results from regional  
450 analyses also broadly overlap with our findings (Da-Allada et al., 2020; Mousavi et al., 2023).  
451 However, Xie et al. (2022) used a 6-model ensemble to identify the impacts of SAI on the Atlantic  
452 Meridional Overturning Circulation and report changes in global wind speed patterns as a result  
453 of SAI that are different from ours. The divergence in results may be partially explained by the  
454 difference in scenario comparisons but it nevertheless suggests that the impacts of SAI on wind  
455 are not well understood to date. The scenario-comparisons in Figure 4 and 5 suggest that SAI does  
456 not compensate for changes from global warming but modifies wind resources in a novel way.

457 While no studies exist to date that evaluate wind energy potential changes under SRM,  
458 studies looking at changes in WRE potential due to climate change have found regionally highly  
459 diverse trends (e.g. Gernaat et al., 2021; Solaun & Cerdá, 2019; Tobin et al., 2015). We generally  
460 see similar developments for the SSP245 and SSP585 comparison as other studies that look at  
461 wind potential under climate change. Remarkable similarities exist on the South American (De  
462 Jong et al., 2019; Gernaat et al., 2021; Pereira De Lucena et al., 2010; Pereira et al., 2013) and  
463 African continent (Gernaat et al., 2021; Sawadogo et al., 2021) and Europe (Carvalho et al., 2017;  
464 Davy et al., 2018; Gernaat et al., 2021; Tobin et al., 2015, 2018).

465 Gernaat et al. (2021) note a relative global reduction in offshore wind potential of 2.1 % from  
466 historical (1970-2000) values to the end of the century under an RCP6.0 pathway and a reduction  
467 in onshore potential by 4.1 %. This is much higher than what we see for SSP245 versus SSP585,  
468 which has a global mean reduction in onshore wind potential of 0.6 % and an increase in offshore  
469 potential of 0.6 %. Our analyses are not directly comparable due to differences in underlying data  
470 and methodology and because our pathways result in a greater level of warming at the point of  
471 comparison. However, the absolute temperature difference between SSP245 and SSP585 and  
472 Gernaat et al.'s historical and end-of-century value is of similar range. Despite the much smaller  
473 relative global change in potential with climate change compared to Gernaat et al.'s study, we  
474 calculate a total global potential that is broadly comparable with the results from Gernaat et al. and  
475 other studies that provide wind technical potential in energy units (Table 2; Archer & Jacobson,  
476 2005; Bosch et al., 2017; Chu & Hawkes, 2020; Eureka et al., 2017; Gernaat et al., 2021; Hoogwijk,

477 2004; de Vries et al., 2007; Lu et al., 2009; Krewitt et al., 2009). Discrepancies are possible due to  
 478 differences in the underlying models, unlike methodological approaches in calculating the  
 479 potential, such as dissimilar assumptions regarding land suitability and the characteristics of the  
 480 wind turbines, as well as the temporal resolution of the wind data. Contrary to those studies, our  
 481 offshore potential is much greater than onshore, and energy losses offshore are also much higher  
 482 than onshore (Figure 7). This is due to the stronger suitability constraints we apply on land grid  
 483 cells and, as demonstrated by Martinez & Iglesias (2024) and Tian et al. (2019), the generally  
 484 higher energy density offshore.

485 **Table 2.** Comparison of total global on- and offshore wind potential with previous studies. Our  
 486 results: SSP245 in 2090-2099 based on yearly sums of hourly output. NA means not available.

	<b>Onshore</b> [PWh/yr]	<b>Offshore</b> [PWh/yr]	<b>Area</b>	<b>Year</b>
<b>Our results</b>	217	399	global	2090-2099
<b>Hoogwijk, 2004</b>	96	NA	global	2000
<b>de Vries et al., 2007</b>	34	NA	global	2000 / 2050
<b>Krewitt et al., 2009</b>	105	16	global	2050
<b>Eurek et al., 2017</b>	560	315	global	NA
<b>Chu &amp; Hawkes, 2020</b>	211	216	global	NA
<b>Bosch et al., 2017</b>	587	330	global	NA
<b>Lu et al., 2009</b>	690	157	global	2000
<b>Archer &amp; Jacobson, 2005</b>	630	NA	global	2000
<b>Gernaat et al., 2021</b>	149	114	global	2070-2100

487  
 488 The LEW metric assesses whether an area encounters notably low weekly energy production  
 489 variations, tackling the intermittency apprehension of RE. Extended durations of considerably low  
 490 production, as measured by the LEW metric, may be more significant than a minor decline from  
 491 high production days to medium production days, as indicated by long-term average data. Several  
 492 areas all over the globe see up to 6 additional or 6 fewer LEWs per year on average under SAI  
 493 than the SSP-scenarios (Figure 6). The regional sign and magnitude of change mostly overlaps  
 494 with that from the 10-year average changes (Figure S10). Baur et al. (2023) computed the LEW  
 495 metric for Photovoltaic potential under SAI and found much larger increases in the order of up to

496 12 additional LEWs per year under SAI compared to SSP245 and less agreement on the sign and  
497 magnitude of change between long-term average and LEW difference. While their change in  
498 LEWs is much higher than what we see for wind, their relative decrease in long-term averages is  
499 much lower. This means that in those weeks where energy production is low for wind RE, it is  
500 particularly low, pulling the long-term average to higher numbers. Whereas for Photovoltaic  
501 potential, the LEWs are frequent but not as unproductive. Since long periods of calm winds or  
502 cloudy conditions can be problematic for energy systems that rely on wind or solar RE, it is  
503 relevant to look at whether regions with high general wind potential and high LEW increase  
504 correlate with regions of high solar potential and high solar LEW increase or trends in other types  
505 of intermittent renewable energies.

506 Wind turbine energy output does not scale linearly with wind speed. Rather, they have a  
507 delicate range of wind speeds in which they can produce electricity, described by the wind turbine  
508 power curve. Hence, lower (higher) wind speeds do not necessarily imply lower (higher) wind  
509 potential. Nevertheless, in our analysis, with the same time periods considered, the maps of  
510 differences in wind potential (Figure S9) correlate well (correlation coefficient 0.68 for SAI; 0.70  
511 for the SSP-scenarios) with the maps of differences in wind speed (Figure 4). However, while total  
512 global potential is smaller under SAI than in the SSP-scenarios, SAI reduces the amount of energy  
513 that is lost due to fast winds that are not harvested by wind turbines (Fig 7). The observed decrease  
514 in WRE potential under SAI can therefore not be attributed to alterations in fast wind patterns and  
515 the current quest for wind turbines with ever-higher cut-out thresholds might take up a lower  
516 priority in an SAI-modified world. The total amount of energy lost due to fast winds for all three  
517 scenarios in our results is likely to be smaller than real-world applications would suggest, partly  
518 due to the Weibull distribution we apply to power output to represent variations in wind speed  
519 over time and space. This distribution results in power outputs for 1-hour average wind speeds that  
520 are above the cut-out wind speed (Fig S2), because even if the average wind speed is above the  
521 cut-out threshold, some samples of the Weibull distribution of that average wind speed may be  
522 below the cut-out and therefore produce electricity. In reality, however, the wind turbines are not  
523 instantly turned on and off for wind gusts above or below the cut-out threshold. This means that  
524 we could be overestimating the energy gained and underestimating the energy lost from fast winds.  
525 However, the wind turbine power curve represents the power output of a single turbine, and our  
526 positively-skewed normal distribution of power output may a better representation of the output

527 from an entire grid cell, as other studies have shown (Bosch et al., 2017; Pryor & Barthelmie,  
528 2010).

529 Wind varies greatly in space and time (Cradden et al., 2014; Lee et al., 2018; Yan et al., 2020) and  
530 our hourly input data, which represents entire 1° grid cells, is not able to fully reflect that. We  
531 regridded our wind data using a bilinear method to match the spatial resolution of the land use data  
532 rather than conducting a costly statistical downscaling. As an approximation of the different wind  
533 speeds in space and time we applied a Weibull distribution. A constant Weibull shape parameter  
534 was used across the globe to ensure computational practicality. However, this approach may lead  
535 to under- or overestimation of wind power output in certain regions (Zhou & Smith, 2013).  
536 Selecting a constant shape parameter in the Weibull distribution is a simplification because it  
537 ultimately relies on the regional wind system and terrain. Nevertheless, any errors that may be  
538 produced from this simplification will affect all three scenarios equally and will be largely negated  
539 when comparing the scenarios. Our study focuses on the impact of SAI on wind renewable energy  
540 potential, specifically differences in predicted future states rather than precise and accurate  
541 regional representations of wind potential.

542 The study's findings are specific to a single SAI experimental set-up (continuous injection  
543 of sulfate aerosols) and model that may have a larger SAI signal than is currently considered in a  
544 hypothetical deployment scenario but allows us a larger signal-to-noise ratio. Since no other  
545 modeling groups have performed SAI experiments with hourly wind output, the study's robustness  
546 is constrained by these limitations. However, several studies looking at surface wind speed changes  
547 under SAI have found similar patterns to us (Da-Allada et al., 2020; Mousavi et al., 2023; Tang et  
548 al., 2023). To increase the robustness of the results, more model intercomparison studies such as  
549 Xie et al.'s 2022 study will need to be performed, as well as different SAI experiment designs.

550 Not all regions have signal-to-noise ratios that are above 1 (Fig S9) or show statistically significant  
551 differences between scenarios (Fig 5, S10), which is a common occurrence for sensitive variables  
552 such as wind. Despite the ongoing debate surrounding the consistency of Global Circulation  
553 Models with observations and their ability to simulate long-term trends (Pryor & Barthelmie, 2010;  
554 Pryor et al., 2020; Tian et al., 2019; Sheperd, 2014), particularly in coastal areas (Soares et al.,  
555 2017; Solaun & Cerdá, 2019), they are presently the most reliable source for global wind  
556 projections with SAI.

557 Our offshore energy assessment may further incur inaccuracies as a result of overestimating  
558 suitable areas by ignoring common shipping lanes and their unsuitability for wind farms. It is likely  
559 that for energy generation purposes unsuitable areas such as ports and frequently used  
560 transportation routes are located in proximity to areas that we consider particularly suitable, that  
561 is, areas close to population centers.

562 This study looks at the large-scale changes in the dynamics of the circulation system. While these  
563 have an important influence on local wind conditions, wind speeds in the lower levels of the  
564 atmospheric boundary layer, i.e., those accessible to wind turbines, are highly susceptible to  
565 turbulence from small-scale features such as buildings, trees and valleys (Veers et al., 2019). These  
566 microscale processes are not resolved in our global analysis. An SSP245-world would likely have  
567 substantial differences in terms of land cover and population distribution compared to an SSP585-  
568 or an SAI-world. As these things are hard to predict and would complicate the comparison between  
569 scenarios, we chose equal area weighting for all scenarios.

570 Future research should not only consider other types of renewable energy sources such as  
571 biofuels and hydropower but look at the effects of SAI on renewable energy sources in conjunction.  
572 This would allow to identify regions where not just one RE technology, but potentially several,  
573 may experience a change in their productivity with SAI. Additionally, it is relevant to consider not  
574 only resource changes due to SRM but also demand changes. One could imagine a modified  
575 demand for heating and cooling under SRM, for example. Studies looking at other types of SRM,  
576 such as Marine Cloud Brightening, would offer a more complete picture on SRM and renewable  
577 energy. At the same time, improvements in the representation of SRM and the response of  
578 atmospheric circulation to a change in forcing in the Earth System Models would substantially  
579 increase accuracy of the results. Since stratospheric heating has been found to play an important  
580 role in changing large-scale circulation (Simpson et al., 2019; Charlesworth et al., 2023, Baldwin  
581 & Dunkerton, 2001; Graft et al., 1993; Stenchikov et al. 2002; DallaSanta et al., 2019), narrowing  
582 down the uncertainty related to the radiative properties of stratospheric aerosols could improve the  
583 understanding of the impacts of SAI on wind RE. And lastly, since SAI seems to significantly  
584 affect the spatial distribution of wind resources, regional scale analyses are an essential addition  
585 in better understanding wind potential under SAI.

586

## 587 **5 Conclusion**

588 Wind renewable energy is considered a critical component in the efforts to reduce  
589 greenhouse gas emissions and transition to a more sustainable energy system. Studying the  
590 interplay between SAI and wind energy is important to understand whether mitigation and SAI  
591 could work together to address climate change. Here, we examined the alterations in wind patterns  
592 and RE resources under SAI using the CNRM-ESM2-1.

593 We find that SAI, while counterbalancing the temperature increase of climate change, does not  
594 seem to counterbalance the effects of climate change on wind RE. Instead, our model simulations  
595 suggest that SAI may create new atmospheric circulation features (Fig 2-4). The overall long-term  
596 impact on WRE resources appears to be highly location-specific, with large increases and  
597 reductions in potential under SAI compared to SSP245 or SSP585 of 16 % (Fig 5, S10). However,  
598 the long-term total global change in potential is negligible. Furthermore, we find that SAI increases  
599 the number of weeks of considerably low production per year in most places around the world (Fig  
600 6) compared to the SSP-scenarios and to the present, although to a much lesser degree than for  
601 solar RE (Baur et al., 2023). We note that the reduction in long-term potential and the increase in  
602 low energy weeks is not due to an increase of wind speed under SAI (Fig 7).

603 This paper contributes to the ongoing discourse on climate intervention strategies and their  
604 implications for mitigation. While this study entails a high temporal resolution and a fairly high  
605 number of ensemble members, future studies could rely on higher spatial resolution models and a  
606 larger range of emission scenarios with SAI to test and improve accuracy of the current  
607 assumptions. Climate projections are still faced with the challenge of understanding the effect of  
608 global warming on atmospheric circulation change and pattern formation (Shepherd, 2014).  
609 Improvements in these fundamental understandings might help in attributing the changes from the  
610 combined effects of global warming and SAI on wind allowing for a better investigation of the  
611 impacts of SAI on WRE potential. We suggest that further research is necessary to assess the wider  
612 impacts of SAI on renewable energies to enable more responsible and informed decision-making  
613 on climate intervention.

614

615

## 616 **Acknowledgments**

617 Susanne Baur is supported by CERFACS through the project MIRAGE. BS and RS

618 acknowledges funding by the European Union's Horizon 2020 (H2020) research and innovation

619 program under Grant Agreement No. 101003536 (ESM2025 – Earth System Models for the  
620 Future), 821003 (4C, Climate-Carbon Interactions in the Coming Century) and 101003687  
621 (PROVIDE).

622

### 623 **Conflict of Interest**

624 The authors declare no conflict of interest.

625

### 626 **Open Research**

#### 627 **Availability Statement**

628 The code is available at [https://github.com/susannebaur/SRM\\_wind\\_RE.git](https://github.com/susannebaur/SRM_wind_RE.git). Upon final  
629 publication the code will be made publicly available with a DOI under zenodo.

630 Underlying data is output from the CNRM-ESM2-1 Earth System Model. Due to the large size of  
631 the raw data (>1.5TB) it is available upon request from the authors until a sufficiently large storage  
632 repository has been found. The post-processed model output will be made available upon final  
633 publication with a DOI on zenodo. Land use and land cover as well as population density  
634 projections are from the IMAGE3.0-LPJ model (Doelman et al., 2018; Stehfest et al., 2014). Land  
635 and ocean protected areas are from the International Union for Conservation of Nature (IUCN,  
636 2023). The Exclusive Economic Zone (EEZ) is from the Flanders Marine Institute (2019),  
637 bathymetry and sea-ice information is output from the CNRM-ESM2-1 simulations. Figures were  
638 created using the matplotlib library and the matplotlib wrapper proplot.

639

### 640 **References**

641 Alizadeh, M. J., Kavianpour, M. R., Kamranzad, B., & Etemad-Shahidi, A. (2020). A distributed  
642 wind downscaling technique for wave climate modeling under future scenarios. *Ocean*  
643 *Modelling*, 145, 101513. <https://doi.org/10.1016/j.ocemod.2019.101513>

- 644 Archer, C. L., & Jacobson, M. Z. (2005). Evaluation of global wind power. *Journal of*  
645 *Geophysical Research: Atmospheres*, *110*(D12), 2004JD005462.  
646 <https://doi.org/10.1029/2004JD005462>
- 647 Arent, D., Sullivan, P., Heimiller, D., Lopez, A., Eurek, K., Badger, J., Jorgensen, H.E., Kelly,  
648 M., Clarke, L., Luckow, P. (2012). Improved offshore wind resource assessment in global  
649 climate stabilization scenarios. NREL/TP-6A20-55049. National Renewable Energy  
650 Laboratory, Golden, CO.
- 651 Aukitino, T., Khan, M. G. M., & Ahmed, M. R. (2017). Wind energy resource assessment for  
652 Kiribati with a comparison of different methods of determining Weibull parameters.  
653 *Energy Conversion and Management*, *151*, 641–660.  
654 <https://doi.org/10.1016/j.enconman.2017.09.027>
- 655 Baldwin, M. P., & Dunkerton, T. J. (2001). Stratospheric Harbingers of Anomalous Weather  
656 Regimes, *294*.
- 657 Barnes, E. A., Solomon, S., & Polvani, L. M. (2016). Robust Wind and Precipitation Responses  
658 to the Mount Pinatubo Eruption, as Simulated in the CMIP5 Models. *Journal of Climate*,  
659 *29*(13), 4763–4778. <https://doi.org/10.1175/JCLI-D-15-0658.1>
- 660 Baur, S., Sanderson, B. M., Séférian, R., & Terray, L. (2023). Solar Radiation Modification  
661 challenges decarbonization with renewable solar energy (preprint). *Earth System*  
662 *Dynamics*. <https://doi.org/10.5194/egusphere-2023-2337>.
- 663 Bosch, J., Staffell, I., & Hawkes, A. D. (2017). Temporally-explicit and spatially-resolved global  
664 onshore wind energy potentials. *Energy*, *131*, 207–217.  
665 <https://doi.org/10.1016/j.energy.2017.05.052>
- 666 Burton, T., Sharpe, D., Jenkins, N., Bossanyi, E. (2001). Wind energy handbook. *John Wiley &*  
667 *Sons*. DOI:10.1002/0470846062
- 668 Carrillo, C., Obando Montaña, A. F., Cidrás, J., & Díaz-Dorado, E. (2013). Review of power  
669 curve modelling for wind turbines. *Renewable and Sustainable Energy Reviews*, *21*, 572–  
670 581. <https://doi.org/10.1016/j.rser.2013.01.012>
- 671 Carvalho, D., Rocha, A., Gómez-Gesteira, M., & Silva Santos, C. (2017). Potential impacts of  
672 climate change on European wind energy resource under the CMIP5 future climate  
673 projections. *Renewable Energy*, *101*, 29–40. <https://doi.org/10.1016/j.renene.2016.08.036>
- 674 Chang, T.-J., Chen, C.-L., Tu, Y.-L., Yeh, H.-T., & Wu, Y.-T. (2015). Evaluation of the climate  
675 change impact on wind resources in Taiwan Strait. *Energy Conversion and Management*,  
676 *95*, 435–445. <https://doi.org/10.1016/j.enconman.2015.02.033>
- 677 Charlesworth, E., Plöger, F., Birner, T., Baikhadzhaev, R., Abalos, M., Abraham, N. L., et al.  
678 (2023). Stratospheric water vapor affecting atmospheric circulation. *Nature*  
679 *Communications*, *14*(1), 3925. <https://doi.org/10.1038/s41467-023-39559-2>
- 680 Cheng, W., MacMartin, D. G., Dagon, K., Kravitz, B., Tilmes, S., Richter, J. H., et al. (2019).  
681 Soil Moisture and Other Hydrological Changes in a Stratospheric Aerosol  
682 Geoengineering Large Ensemble. *Journal of Geophysical Research: Atmospheres*,  
683 *124*(23), 12773–12793. <https://doi.org/10.1029/2018JD030237>
- 684 Chu, C.-T., & Hawkes, A. D. (2020). A geographic information system-based global variable  
685 renewable potential assessment using spatially resolved simulation. *Energy*, *193*, 116630.  
686 <https://doi.org/10.1016/j.energy.2019.116630>
- 687 Clarke, L., Wei, Y.-M., De La Vega Navarro, A., Garg, A., Hahmann, A.N., Khennas, S.,  
688 Azevedo, I.M.L., Löschel, A., Singh, A.K., Steg, L., Strbac, G., Wada, K. (2022). Energy  
689 Systems. In IPCC, 2022: Climate Change 2022: Mitigation of Climate Change.

- 690 Contribution of Working Group III to the Sixth Assessment Report of the  
691 Intergovernmental Panel on Climate Change [P.R. Shukla, J. Skea, R. Slade, A. Al  
692 Khourdajie, R. van Diemen, D. McCollum, M. Pathak, S. Some, P. Vyas, R. Fradera, M.  
693 Belkacemi, A. Hasija, G. Lisboa, S. Luz, J. Malley, (eds.)]. *Cambridge University Press,*  
694 *Cambridge, UK and New York, NY, USA.* doi: 10.1017/9781009157926.008
- 695 Cradden, L., Restuccia, F., Hawkins, S., & Harrison, G. (2014). Consideration of Wind Speed  
696 Variability in Creating a Regional Aggregate Wind Power Time Series. *Resources*, 3(1),  
697 215–234. <https://doi.org/10.3390/resources3010215>
- 698 Da-Allada, C. Y., Baloïtcha, E., Alamou, E. A., Awo, F. M., Bonou, F., Pomalegni, Y., et al.  
699 (2020). Changes in West African Summer Monsoon Precipitation Under Stratospheric  
700 Aerosol Geoengineering. *Earth's Future*, 8(7), e2020EF001595.  
701 <https://doi.org/10.1029/2020EF001595>
- 702 Dai, Z., Weisenstein, D. K., & Keith, D. W. (2018). Tailoring Meridional and Seasonal Radiative  
703 Forcing by Sulfate Aerosol Solar Geoengineering. *Geophysical Research Letters*, 45(2),  
704 1030–1039. <https://doi.org/10.1002/2017GL076472>
- 705 DallaSanta, K., Gerber, E. P., & Toohey, M. (2019). The Circulation Response to Volcanic  
706 Eruptions: The Key Roles of Stratospheric Warming and Eddy Interactions. *Journal of*  
707 *Climate*, 32(4), 1101–1120. <https://doi.org/10.1175/JCLI-D-18-0099.1>
- 708 Davy, R., Gnatiuk, N., Pettersson, L., & Bobylev, L. (2018). Climate change impacts on wind  
709 energy potential in the European domain with a focus on the Black Sea. *Renewable and*  
710 *Sustainable Energy Reviews*, 81, 1652–1659. <https://doi.org/10.1016/j.rser.2017.05.253>
- 711 De Jong, P., Barreto, T. B., Tanajura, C. A. S., Kouloukoui, D., Oliveira-Esquerre, K. P.,  
712 Kiperstok, A., & Torres, E. A. (2019). Estimating the impact of climate change on wind  
713 and solar energy in Brazil using a South American regional climate model. *Renewable*  
714 *Energy*, 141, 390–401. <https://doi.org/10.1016/j.renene.2019.03.086>
- 715 Doelman, J. C., Stehfest, E., Tabeau, A., Van Meijl, H., Lassaletta, L., Gernaat, D. E. H. J., et al.  
716 (2018). Exploring SSP land-use dynamics using the IMAGE model: Regional and  
717 gridded scenarios of land-use change and land-based climate change mitigation. *Global*  
718 *Environmental Change*, 48, 119–135. <https://doi.org/10.1016/j.gloenvcha.2017.11.014>
- 719 Dvorak, M. J., Archer, C. L., & Jacobson, M. Z. (2010). California offshore wind energy  
720 potential. *Renewable Energy*, 35(6), 1244–1254.  
721 <https://doi.org/10.1016/j.renene.2009.11.022>
- 722 Elliot, D., Schwartz, M. (1993). Wind energy potential in the United States. *Pacific Northwest*  
723 *Laboratory*.
- 724 Elsner, P. (2019). Continental-scale assessment of the African offshore wind energy potential:  
725 Spatial analysis of an under-appreciated renewable energy resource. *Renewable and*  
726 *Sustainable Energy Reviews*, 104, 394–407. <https://doi.org/10.1016/j.rser.2019.01.034>
- 727 Eskin, N., Artar, H., & Tolun, S. (2008). Wind energy potential of Gökçeada Island in Turkey.  
728 *Renewable and Sustainable Energy Reviews*, 12(3), 839–851.  
729 <https://doi.org/10.1016/j.rser.2006.05.016>
- 730 Eurek, K., Sullivan, P., Gleason, M., Hettinger, D., Heimiller, D., & Lopez, A. (2017). An  
731 improved global wind resource estimate for integrated assessment models. *Energy*  
732 *Economics*, 64, 552–567. <https://doi.org/10.1016/j.eneco.2016.11.015>
- 733 Flanders Marine Institute (2019). Maritime Boundaries Geodatabase: Maritime Boundaries and  
734 Exclusive Economic Zones (200NM), version 11. Available online at  
735 <https://www.marineregions.org/>. Last accessed: 05. April 2023.

- 736 Gernaat, D. E. H. J., de Boer, H. S., Daioglou, V., Yalew, S. G., Müller, C., & van Vuuren, D. P.  
737 (2021). Climate change impacts on renewable energy supply. *Nature Climate Change*,  
738 *11*(2), 119–125. <https://doi.org/10.1038/s41558-020-00949-9>
- 739 Graf, H.-F. (1992). Arctic radiation deficit and climate variability. *Climate Dynamics*, *7*, 19–28,  
740 <https://doi.org/10.1007/BF00204818>.
- 741 Graft, H.-F., Kirchner, I., Robock, A. (1993). Pinatubo eruption winter climate effects: model  
742 versus observations. *Climate Dynamics*, *9*, 81–93. <https://doi.org/10.1007/BF00210011>
- 743 Hoogwijk, M. M. (2004). *On the global and regional potential of renewable energy sources =*  
744 *Over het mondiale en regionale potentieel van hernieuwbare energiebronnen*.  
745 Universiteit Utrecht, Faculteit Scheikunde, Utrecht.
- 746 Horton, J. B. (2015). The emergency framing of solar geoengineering: Time for a different  
747 approach. *The Anthropocene Review*, *2*(2), 147–151.  
748 <https://doi.org/10.1177/2053019615579922>
- 749 IPCC (2018). Summary for Policymakers. In: Global Warming of 1.5°C. An IPCC Special  
750 Report on the impacts of global warming of 1.5°C above pre-industrial levels and related  
751 global greenhouse gas emission pathways, in the context of strengthening the global  
752 response to the threat of climate change, sustainable development, and efforts to eradicate  
753 poverty [Masson-Delmotte, V., P. Zhai, H.-O. Pörtner, D. Roberts, J. Skea, P.R. Shukla,  
754 A. Pirani, W. Moufouma-Okia, C. Péan, R. Pidcock, S. Connors, J.B.R. Matthews, Y.  
755 Chen, X. Zhou, M.I. Gomis, E. Lonnoy, T. Maycock, M. Tignor, and T. Waterfield  
756 (eds.)]. *Cambridge University Press, Cambridge, UK and New York, NY, USA*, 3-24.  
757 <https://doi.org/10.1017/9781009157940.001>
- 758 IUCN (International Union for Conservation of Nature) (2023). The World Database on  
759 Protected Areas (WDPA).
- 760 Jung, C., & Schindler, D. (2022). A review of recent studies on wind resource projections under  
761 climate change. *Renewable and Sustainable Energy Reviews*, *165*, 112596.  
762 <https://doi.org/10.1016/j.rser.2022.112596>
- 763 Jung, C., Schindler, D., & Laible, J. (2018). National and global wind resource assessment under  
764 six wind turbine installation scenarios. *Energy Conversion and Management*, *156*, 403–  
765 415. <https://doi.org/10.1016/j.enconman.2017.11.059>
- 766 Justus, C.G., Hargraves, W.R., Mikhail, A. & Graber, D. (1978). Methods for estimating wind  
767 speed frequency distributions. *J. Appl. Meteorol.*, *17*, 350–353.
- 768 Karpechko, A. Yu., Gillett, N. P., Dall’Amico, M., & Gray, L. J. (2010). Southern Hemisphere  
769 atmospheric circulation response to the El Chichón and Pinatubo eruptions in coupled  
770 climate models: Southern Hemisphere Response to El Chichón and Pinatubo. *Quarterly*  
771 *Journal of the Royal Meteorological Society*, *136*(652), 1813–1822.  
772 <https://doi.org/10.1002/qj.683>
- 773 Kirchner, I., Stenchikov, G. L., Graf, H.-F., Robock, A. & Antufia, J. C. (1999). Climate model  
774 simulation of winter warming and summer cooling following the 1991 Mount Pinatubo  
775 volcanic eruption. *J. Geophys. Res.*, *104*, 19 039–19 055, [https://](https://doi.org/10.1029/1999JD900213)  
776 [doi.org/10.1029/1999JD900213](https://doi.org/10.1029/1999JD900213).
- 777 Kravitz, B., Robock, A., Tilmes, S., Boucher, O., English, J. M., Irvine, P. J., et al. (2015). The  
778 Geoengineering Model Intercomparison Project Phase 6 (GeoMIP6): Simulation design  
779 and preliminary results. *Geoscientific Model Development*, *8*(10), 3379–3392.  
780 <https://doi.org/10.5194/gmd-8-3379-2015>

- 781 Kravitz, Ben, MacMartin, D. G., Wang, H., & Rasch, P. J. (2016). Geoengineering as a design  
782 problem. *Earth System Dynamics*, 7(2), 469–497. <https://doi.org/10.5194/esd-7-469-2016>
- 783 Kravitz, Ben, MacMartin, D. G., Tilmes, S., Richter, J. H., Mills, M. J., Cheng, W., et al.  
784 (2019a). Comparing Surface and Stratospheric Impacts of Geoengineering With Different  
785 SO<sub>2</sub> Injection Strategies. *Journal of Geophysical Research: Atmospheres*, 124(14),  
786 7900–7918. <https://doi.org/10.1029/2019JD030329>
- 787 Kravitz, Ben, MacMartin, D. G., Tilmes, S., Richter, J. H., Mills, M. J., Cheng, W., et al.  
788 (2019b). Comparing Surface and Stratospheric Impacts of Geoengineering With Different  
789 SO<sub>2</sub> Injection Strategies. *Journal of Geophysical Research: Atmospheres*, 124(14),  
790 7900–7918. <https://doi.org/10.1029/2019JD030329>
- 791 Krewitt, W., K. Nienhaus, C. Kleßmann, C. Capone, E. Stricker, W. Graus, M. Hoogwijk, N.  
792 Supersberger, U. von Winterfeld & Samadi, S. (2009). Role and Potential of Renewable  
793 Energy and Energy Efficiency for Global Energy Supply. *Climate Change*, 18, 336, ISSN  
794 1862-4359, Federal Environment Agency, Dessau-Roßlau, Germany.
- 795 Lee, H., Muri, H., Ekici, A., Tjiputra, J., & Schwinger, J. (2020). The response of terrestrial  
796 ecosystem carbon cycling under different aerosol-based radiation management  
797 geoengineering. *Earth System Dynamics*, (July). <https://doi.org/10.5194/esd-2020-57>
- 798 Lee, J. C. Y., Fields, M. J., & Lundquist, J. K. (2018). Assessing variability of wind speed:  
799 comparison and validation of 27 methodologies. *Wind Energy Science*, 3(2), 845–868.  
800 <https://doi.org/10.5194/wes-3-845-2018>
- 801 Li, Y., Huang, X., Tee, K. F., Li, Q., & Wu, X.-P. (2020). Comparative study of onshore and  
802 offshore wind characteristics and wind energy potentials: A case study for southeast  
803 coastal region of China. *Sustainable Energy Technologies and Assessments*, 39, 100711.  
804 <https://doi.org/10.1016/j.seta.2020.100711>
- 805 Liu, Z., Lang, X., Miao, J., & Jiang, D. (2023). Impact of Stratospheric Aerosol Injection on the  
806 East Asian Winter Monsoon. *Geophysical Research Letters*, 50(3), e2022GL102109.  
807 <https://doi.org/10.1029/2022GL102109>
- 808 Lu, X., M.B. McElroy & Kiviluoma, J. (2009). Global potential for wind-generated electricity.  
809 *Proceedings of the National Academy of Sciences*, 106, 10933- 10939.
- 810 Lysen, E. H. (1983). Introduction to Wind Energy. *CWD Publication, The Netherlands*, No.  
811 CWD 82–1.
- 812 Ma, J., Xie, S.-P., & Kosaka, Y. (2012). Mechanisms for Tropical Tropospheric Circulation  
813 Change in Response to Global Warming\*. *Journal of Climate*, 25(8), 2979–2994.  
814 <https://doi.org/10.1175/JCLI-D-11-00048.1>
- 815 MacCracken, M. C. (2009). On the possible use of geoengineering to moderate specific climate  
816 change impacts. *Environmental Research Letters*, 4(4), 045107.  
817 <https://doi.org/10.1088/1748-9326/4/4/045107>
- 818 MacMartin, D. G., & Kravitz, B. (2019). The Engineering of Climate Engineering. *Annual*  
819 *Review of Control, Robotics, and Autonomous Systems*, 2(1), 445–467.  
820 <https://doi.org/10.1146/annurev-control-053018-023725>
- 821 Marshall, A. G., Scaife, A. A., & Ineson, S. (2009). Enhanced Seasonal Prediction of European  
822 Winter Warming following Volcanic Eruptions. *Journal of Climate*, 22(23), 6168–6180.  
823 <https://doi.org/10.1175/2009JCLI3145.1>
- 824 Martinez, A., & Iglesias, G. (2024). Global wind energy resources decline under climate change.  
825 *Energy*, 288, 129765. <https://doi.org/10.1016/j.energy.2023.129765>

- 826 McCusker, K. E., Battisti, D. S., & Bitz, C. M. (2015). Inability of stratospheric sulfate aerosol  
827 injections to preserve the West Antarctic Ice Sheet. *Geophysical Research Letters*,  
828 42(12), 4989–4997. <https://doi.org/10.1002/2015GL064314>
- 829 McCusker, Kelly E., Armour, K. C., Bitz, C. M., & Battisti, D. S. (2014). Rapid and extensive  
830 warming following cessation of solar radiation management. *Environmental Research*  
831 *Letters*, 9(2). <https://doi.org/10.1088/1748-9326/9/2/024005>
- 832 McGraw, M. C., Barnes, E. A., & Deser, C. (2016). Reconciling the observed and modeled  
833 Southern Hemisphere circulation response to volcanic eruptions. *Geophysical Research*  
834 *Letters*, 43(13), 7259–7266. <https://doi.org/10.1002/2016GL069835>
- 835 Mohammadi, K., Alavi, O., Mostafaeipour, A., Goudarzi, N., & Jalilvand, M. (2016). Assessing  
836 different parameters estimation methods of Weibull distribution to compute wind power  
837 density. *Energy Conversion and Management*, 108, 322–335.  
838 <https://doi.org/10.1016/j.enconman.2015.11.015>
- 839 Mousavi, S. V., Karami, K., Tilmes, S., Muri, H., Xia, L., & Rezaei, A. (2023). Future dust  
840 concentration over the Middle East and North Africa region under global warming and  
841 stratospheric aerosol intervention scenarios. *Atmospheric Chemistry and Physics*, 23(18),  
842 10677–10695. <https://doi.org/10.5194/acp-23-10677-2023>
- 843 Müller-Hansen, F., Repke, T., Baum, C. M., Brutschin, E., Callaghan, M. W., Debnath, R., et al.  
844 (2023). Attention, sentiments and emotions towards emerging climate technologies on  
845 Twitter. *Global Environmental Change*, 83, 102765.  
846 <https://doi.org/10.1016/j.gloenvcha.2023.102765>
- 847 O'Neill, B. C., Tebaldi, C., Van Vuuren, D. P., Eyring, V., Friedlingstein, P., Hurtt, G., et al.  
848 (2016). The Scenario Model Intercomparison Project (ScenarioMIP) for CMIP6.  
849 *Geoscientific Model Development*, 9(9), 3461–3482. [https://doi.org/10.5194/gmd-9-3461-](https://doi.org/10.5194/gmd-9-3461-2016)  
850 2016
- 851 Pereira De Lucena, A. F., Szklo, A. S., Schaeffer, R., & Dutra, R. M. (2010). The vulnerability  
852 of wind power to climate change in Brazil. *Renewable Energy*, 35(5), 904–912.  
853 <https://doi.org/10.1016/j.renene.2009.10.022>
- 854 Pereira, E. B., Martins, F. R., Pes, M. P., Da Cruz Segundo, E. I., & Lyra, A. D. A. (2013). The  
855 impacts of global climate changes on the wind power density in Brazil. *Renewable*  
856 *Energy*, 49, 107–110. <https://doi.org/10.1016/j.renene.2012.01.053>
- 857 Perrin, O., Rootzén, H., & Taesler, R. (2006). A Discussion of Statistical Methods Used to  
858 Estimate Extreme Wind Speeds. *Theor. Appl. Climatol*, 85(3-4), 203–215.  
859 [doi:10.1007/s00704-005-0187-3](https://doi.org/10.1007/s00704-005-0187-3)
- 860 Polvani, L. M., & Kushner, P. J. (2002). Tropospheric response to stratospheric perturbations in  
861 a relatively simple general circulation model. *Geophysical Research Letters*, 29(7).  
862 <https://doi.org/10.1029/2001GL014284>
- 863 Pryor, S. C., Nielsen, M., Barthelmie, R. J. & Mann, J. (2004). Can satellite sampling of offshore  
864 wind speeds realistically represent wind speed distributions? Part II: Quantifying  
865 uncertainties associated with sampling strategy and distribution fitting methods. *J. Appl.*  
866 *Meteorol.*, 43, 739–750.
- 867 Pryor, S.C., R.J. Barthelmie, D.T. Young, E.S. Takle, R.W. Arritt, D. Flory, W. Gutowski Jr., A.  
868 Nunes & Roads, J. (2009). Wind speed trends over the contiguous United States. *Journal*  
869 *of Geophysical Research – Atmospheres*, 114, D14105.

- 870 Pryor, S. C., & Barthelmie, R. J. (2010). Climate change impacts on wind energy: A review.  
871 *Renewable and Sustainable Energy Reviews*, *14*(1), 430–437.  
872 <https://doi.org/10.1016/j.rser.2009.07.028>
- 873 Pryor, S. C., Barthelmie, R. J., Bukovsky, M. S., Leung, L. R., & Sakaguchi, K. (2020). Climate  
874 change impacts on wind power generation. *Nature Reviews Earth & Environment*, *1*(12),  
875 627–643. <https://doi.org/10.1038/s43017-020-0101-7>
- 876 Ramachandran, S., Ramaswamy, V., Stenchikov, G. L., & Robock, A. (2000). Radiative impact  
877 of the Mount Pinatubo volcanic eruption: Lower stratospheric response. *Journal of*  
878 *Geophysical Research: Atmospheres*, *105*(D19), 24409–24429.  
879 <https://doi.org/10.1029/2000JD900355>
- 880 Riahi, K., Schaeffer, R., Arango, J., Calvin, K., Guivarch, C., Hasegawa, T., Jiang, K., Kriegler,  
881 E., Matthews, R., Peters, G.P., Rao, A., Robertson, S., Sebbit, A.M., Steinberger, J.,  
882 Tavoni, M., van Vuuren, D.P. (2022). Mitigation pathways compatible with long-term  
883 goals. In IPCC, 2022: Climate Change 2022: Mitigation of Climate Change. Contribution  
884 of Working Group III to the Sixth Assessment Report of the Intergovernmental Panel on  
885 Climate Change [P.R. Shukla, J. Skea, R. Slade, A. Al Khourdajie, R. van Diemen, D.  
886 McCollum, M. Pathak, S. Some, P. Vyas, R. Fradera, M. Belkacemi, A. Hasija, G.  
887 Lisboa, S. Luz, J. Malley, (eds.)]. *Cambridge University Press, Cambridge, UK and New*  
888 *York, NY, USA*. doi: 10.1017/9781009157926.005
- 889 Ripple, W. J., Wolf, C., Gregg, J. W., Rockström, J., Newsome, T. M., Law, B. E., et al. (2023).  
890 The 2023 state of the climate report: Entering uncharted territory. *BioScience*, *73*(12),  
891 841–850. <https://doi.org/10.1093/biosci/biad080>
- 892 Robock, A., Adams, T., Moore, M., Oman, L., & Stenchikov, G. (2007). Southern Hemisphere  
893 atmospheric circulation effects of the 1991 Mount Pinatubo eruption. *Geophysical*  
894 *Research Letters*, *34*(23), 2007GL031403. <https://doi.org/10.1029/2007GL031403>
- 895 Robock, A., Oman, L., & Stenchikov, G. L. (2008). Regional climate responses to  
896 geoengineering with tropical and Arctic SO<sub>2</sub> injections. *Journal of Geophysical Research*  
897 *Atmospheres*, *113*(16), 1–15. <https://doi.org/10.1029/2008JD010050>
- 898 Roscoe, H. K., & Haigh, J. D. (2007). Influences of ozone depletion, the solar cycle and the  
899 QBO on the Southern Annular Mode: INFLUENCES ON THE SOUTHERN  
900 ANNULAR MODE. *Quarterly Journal of the Royal Meteorological Society*, *133*(628),  
901 1855–1864. <https://doi.org/10.1002/qj.153>
- 902 Royal Society. (2011). *Solar Radiation Management: The Governance of Research* (p. 70).  
903 London, UK: The Royal Society of London. Retrieved from [https://royalsociety.org/-](https://royalsociety.org/-/media/Royal_Society_Content/policy/projects/solar-radiation-governance/DES2391_SRMGI-report_web.pdf)  
904 [/media/Royal\\_Society\\_Content/policy/projects/solar-radiation-](https://royalsociety.org/-/media/Royal_Society_Content/policy/projects/solar-radiation-governance/DES2391_SRMGI-report_web.pdf)  
905 [governance/DES2391\\_SRMGI-report\\_web.pdf](https://royalsociety.org/-/media/Royal_Society_Content/policy/projects/solar-radiation-governance/DES2391_SRMGI-report_web.pdf)
- 906 Saint-Drenan, Y.-M., Besseau, R., Jansen, M., Staffell, I., Troccoli, A., Dubus, L., et al. (2020).  
907 A parametric model for wind turbine power curves incorporating environmental  
908 conditions. *Renewable Energy*, *157*, 754–768.  
909 <https://doi.org/10.1016/j.renene.2020.04.123>
- 910 Sawadogo, W., Reboita, M. S., Faye, A., da Rocha, R. P., Odoulami, R. C., Olusegun, C. F., et  
911 al. (2021). Current and future potential of solar and wind energy over Africa using the  
912 RegCM4 CORDEX-CORE ensemble. *Climate Dynamics*, *57*(5), 1647–1672.  
913 <https://doi.org/10.1007/s00382-020-05377-1>

- 914 Schäfer, S., Stelzer, H., Maas, A., & Lawrence, M. G. (2014). Earth's future in the  
915 Anthropocene: Technological interventions between piecemeal and utopian social  
916 engineering. *Earth's Future*, 2(4), 239–243. <https://doi.org/10.1002/2013EF000190>
- 917 Séférian, R., Nabat, P., Michou, M., Saint-Martin, D., Voldoire, A., Colin, J., et al. (2019).  
918 Evaluation of CNRM Earth System Model, CNRM-ESM2-1: Role of Earth System  
919 Processes in Present-Day and Future Climate. *Journal of Advances in Modeling Earth*  
920 *Systems*, 11(12), 4182–4227. <https://doi.org/10.1029/2019MS001791>
- 921 Shaw, T. A., Baldwin, M., Barnes, E. A., Caballero, R., Garfinkel, C. I., Hwang, Y.-T., et al.  
922 (2016). Storm track processes and the opposing influences of climate change. *Nature*  
923 *Geoscience*, 9(9), 656–664. <https://doi.org/10.1038/ngeo2783>
- 924 Shepherd, T. (2014). Atmospheric circulation as a source of uncertainty in climate change  
925 projections. *Nature Geosci.*, 7, 703–708. [https://doi-](https://doi-org.insu.bib.cnrs.fr/10.1038/ngeo2253)  
926 [org.insu.bib.cnrs.fr/10.1038/ngeo2253](https://doi-org.insu.bib.cnrs.fr/10.1038/ngeo2253)
- 927 Shi, H., Dong, Z., Xiao, N., & Huang, Q. (2021). Wind Speed Distributions Used in Wind  
928 Energy Assessment: A Review. *Frontiers in Energy Research*, 9. Retrieved from  
929 <https://www.frontiersin.org/articles/10.3389/fenrg.2021.769920>
- 930 Shin, J.-Y., Jeong, C., & Heo, J.-H. (2018). A Novel Statistical Method to Temporally  
931 Downscale Wind Speed Weibull Distribution Using Scaling Property. *Energies*, 11(3),  
932 633. <https://doi.org/10.3390/en11030633>
- 933 Shu, Z. R., & Jesson, M. (2021). Estimation of Weibull parameters for wind energy analysis  
934 across the UK. *Journal of Renewable and Sustainable Energy*, 13(2), 023303.  
935 <https://doi.org/10.1063/5.0038001>
- 936 Shu, Z. R., Li, Q. S., & Chan, P. W. (2015). Investigation of offshore wind energy potential in  
937 Hong Kong based on Weibull distribution function. *Applied Energy*, 156, 362–373.  
938 <https://doi.org/10.1016/j.apenergy.2015.07.027>
- 939 Simpson, I. R., Tilmes, S., Richter, J. H., Kravitz, B., MacMartin, D. G., Mills, M. J., et al.  
940 (2019). The Regional Hydroclimate Response to Stratospheric Sulfate Geoengineering  
941 and the Role of Stratospheric Heating. *Journal of Geophysical Research: Atmospheres*,  
942 124(23), 12587–12616. <https://doi.org/10.1029/2019JD031093>
- 943 Simpson, Isla R., Blackburn, M., & Haigh, J. D. (2009). The Role of Eddies in Driving the  
944 Tropospheric Response to Stratospheric Heating Perturbations. *Journal of the*  
945 *Atmospheric Sciences*, 66(5), 1347–1365. <https://doi.org/10.1175/2008JAS2758.1>
- 946 Soares, P. M. M., Lima, D. C. A., Cardoso, R. M., Nascimento, M. L., & Semedo, A. (2017).  
947 Western Iberian offshore wind resources: More or less in a global warming climate?  
948 *Applied Energy*, 203, 72–90. <https://doi.org/10.1016/j.apenergy.2017.06.004>
- 949 Sohoni, V., Gupta, S. C., & Nema, R. K. (2016). A Critical Review on Wind Turbine Power  
950 Curve Modelling Techniques and Their Applications in Wind Based Energy Systems.  
951 *Journal of Energy*, 2016, 1–18. <https://doi.org/10.1155/2016/8519785>
- 952 Solaun, K., & Cerdá, E. (2019). Climate change impacts on renewable energy generation. A  
953 review of quantitative projections. *Renewable and Sustainable Energy Reviews*, 116.  
954 <https://doi.org/10.1016/j.rser.2019.109415>
- 955 Stehfest, E., Van Vuuren, D., Kram, T., Bouwman, L., Alkemade, R., Bakkenes, M., Biemans,  
956 H., Bouwman, A., Den Elzen, M., Janse, J., Lucas, P., Van Minnen, J., Müller, C. &  
957 Prins, A. (2014). Integrated Assessment of Global Environmental Change with IMAGE  
958 3.0. Model Description and Policy Applications, *Netherlands Environmental Assessment*  
959 *Agency (The Hague)*, ISBN: 978-94-91506-71-0

- 960 Stenchikov, G., Robock, A., Ramaswamy, V., Schwarzkopf, M. D., Hamilton, K., &  
961 Ramachandran, S. (2002). Arctic Oscillation response to the 1991 Mount Pinatubo  
962 eruption: Effects of volcanic aerosols and ozone depletion. *Journal of Geophysical*  
963 *Research: Atmospheres*, 107(D24). <https://doi.org/10.1029/2002JD002090>
- 964 Tang, W., Tilmes, S., Lawrence, D. M., Li, F., He, C., Emmons, L. K., et al. (2023). Impact of  
965 solar geoengineering on wildfires in the 21st century in CESM2/WACCM6. *Atmospheric*  
966 *Chemistry and Physics*, 23(9), 5467–5486. <https://doi.org/10.5194/acp-23-5467-2023>
- 967 Tian, Q., Huang, G., Hu, K., & Niyogi, D. (2019). Observed and global climate model based  
968 changes in wind power potential over the Northern Hemisphere during 1979–2016.  
969 *Energy*, 167, 1224–1235. <https://doi.org/10.1016/j.energy.2018.11.027>
- 970 Tilmes, S., Mills, M. J., Niemeier, U., Schmidt, H., Robock, A., Kravitz, B., et al. (2015). A new  
971 Geoengineering Model Intercomparison Project (GeoMIP) experiment designed for  
972 climate and chemistry models. *Geoscientific Model Development*, 8(1), 43–49.  
973 <https://doi.org/10.5194/gmd-8-43-2015>
- 974 Tilmes, Simone, Richter, J. H., Mills, M. J., Kravitz, B., Macmartin, D. G., Vitt, F., et al. (2017).  
975 Sensitivity of aerosol distribution and climate response to stratospheric SO<sub>2</sub> injection  
976 locations. *Journal of Geophysical Research: Atmospheres*, 122(23), 12,591–12,615.  
977 <https://doi.org/10.1002/2017JD026888>
- 978 Tilmes, Simone, Richter, J. H., Kravitz, B., Macmartin, D. G., Mills, M. J., Simpson, I. R., et al.  
979 (2018a). CESM1(WACCM) stratospheric aerosol geoengineering large ensemble project.  
980 *Bulletin of the American Meteorological Society*, 99(11), 2361–2371.  
981 <https://doi.org/10.1175/BAMS-D-17-0267.1>
- 982 Tilmes, Simone, Richter, J. H., Mills, M. J., Kravitz, B., MacMartin, D. G., Garcia, R. R., et al.  
983 (2018b). Effects of Different Stratospheric SO<sub>2</sub> Injection Altitudes on Stratospheric  
984 Chemistry and Dynamics. *Journal of Geophysical Research: Atmospheres*, 123(9), 4654–  
985 4673. <https://doi.org/10.1002/2017JD028146>
- 986 Tobin, I., Greuell, W., Jerez, S., Ludwig, F., Vautard, R., Van Vliet, M. T. H., & Breón, F. M.  
987 (2018). Vulnerabilities and resilience of European power generation to 1.5 °C, 2 °C and 3  
988 °C warming. *Environmental Research Letters*, 13(4). [https://doi.org/10.1088/1748-](https://doi.org/10.1088/1748-9326/aab211)  
989 [9326/aab211](https://doi.org/10.1088/1748-9326/aab211)
- 990 Tobin, Isabelle, Vautard, R., Balog, I., Bréon, F. M., Jerez, S., Ruti, P. M., et al. (2015).  
991 Assessing climate change impacts on European wind energy from ENSEMBLES high-  
992 resolution climate projections. *Climatic Change*, 128(1–2), 99–112.  
993 <https://doi.org/10.1007/s10584-014-1291-0>
- 994 Tye, M. R., Stephenson, D. B., Holland, G. J., & Katz, R. W. (2014). A Weibull Approach for  
995 Improving Climate Model Projections of Tropical Cyclone Wind-Speed Distributions.  
996 *Journal of Climate*, 27(16), 6119–6133. <https://doi.org/10.1175/JCLI-D-14-00121.1>
- 997 Valencia Ochoa, G., Núñez Alvarez, J., & Vanegas Chamorro, M. (2019). Data set on wind  
998 speed, wind direction and wind probability distributions in Puerto Bolivar - Colombia.  
999 *Data in Brief*, 27, 104753. <https://doi.org/10.1016/j.dib.2019.104753>
- 1000 Vautard, R., Cattiaux, J., Yiou, P., Thépaut, J.-N., & Ciais, P. (2010). Northern Hemisphere  
1001 atmospheric stilling partly attributed to an increase in surface roughness. *Nature*  
1002 *Geoscience*, 3(11), 756–761. <https://doi.org/10.1038/ngeo979>
- 1003 Veers, P., Dykes, K., Lantz, E., Barth, S., Bottasso, C. L., Carlson, O., et al. (2019). Grand  
1004 challenges in the science of wind energy. *Science*, 366(6464), eaau2027.  
1005 <https://doi.org/10.1126/science.aau2027>

- 1006 Veronesi, F., & Grassi, S. (2015). Comparison of hourly and daily wind speed observations for  
1007 the computation of Weibull parameters and power output. In *2015 3rd International*  
1008 *Renewable and Sustainable Energy Conference (IRSEC)* (pp. 1–6). Marrakech, Morocco:  
1009 IEEE. <https://doi.org/10.1109/IRSEC.2015.7455043>
- 1010 Vestas (2023a). V236-15.0 MW<sup>TM</sup>. <https://www.vestas.com/en/products/offshore/V236-15MW>.  
1011 Last accessed: 24. January 2024.
- 1012 Vestas (2023b). V162-6.2 MW<sup>TM</sup>. [https://www.vestas.com/en/products/enventus-platform/v162-](https://www.vestas.com/en/products/enventus-platform/v162-6-2-mw)  
1013 [6-2-mw](https://www.vestas.com/en/products/enventus-platform/v162-6-2-mw). Last accessed: 24. January 2024.
- 1014 de Vries, B. J. M., van Vuuren, D. P., & Hoogwijk, M. M. (2007). Renewable energy sources:  
1015 Their global potential for the first-half of the 21st century at a global level: An integrated  
1016 approach. *Energy Policy*, 35(4), 2590–2610. <https://doi.org/10.1016/j.enpol.2006.09.002>
- 1017 Wood, A.J. and Wollenberg, B. (1996) Power Generation Operation and Control. 2nd Edition.  
1018 *Fuel and Energy Abstracts, Elsevier*, 37(3), 195.
- 1019 Xie, M., Moore, J. C., Zhao, L., Wolovick, M., & Muri, H. (2022). Impacts of three types of  
1020 solar geoengineering on the Atlantic Meridional Overturning Circulation. *Atmospheric*  
1021 *Chemistry and Physics*, 22(7), 4581–4597. <https://doi.org/10.5194/acp-22-4581-2022>
- 1022 Yan, B., Chan, P. W., Li, Q. S., He, Y. C., & Shu, Z. R. (2020). Characterising the fractal  
1023 dimension of wind speed time series under different terrain conditions. *Journal of Wind*  
1024 *Engineering and Industrial Aerodynamics*, 201, 104165.  
1025 <https://doi.org/10.1016/j.jweia.2020.104165>
- 1026 Zeng, Z., Ziegler, A.D., Searchinger, T., Yang, L., Chen, A., Ju, K. et al. (2019). A reversal in  
1027 global terrestrial stilling and its implications for wind energy production. *Nat Clim*  
1028 *Change*, 9, 979–85. <https://doi.org/10.1038/s41558-019-0622-6>
- 1029 Zhou, Y., & Smith, S. J. (2013). Spatial and temporal patterns of global onshore wind speed  
1030 distribution. *Environmental Research Letters*, 8(3), 034029. [https://doi.org/10.1088/1748-](https://doi.org/10.1088/1748-9326/8/3/034029)  
1031 [9326/8/3/034029](https://doi.org/10.1088/1748-9326/8/3/034029)
- 1032 Zhou, Y., Luckow, P., Smith, S. J., & Clarke, L. (2012). Evaluation of Global Onshore Wind  
1033 Energy Potential and Generation Costs. *Environmental Science & Technology*, 46(14),  
1034 7857–7864. <https://doi.org/10.1021/es204706m>  
1035